Arabian Journal of Chemistry (2021) **14**, 102905

King Saud University

Arabian Journal of Chemistry

www.ksu.edu.sa
www.sciencedirect.com

ORIGINAL ARTICLE

Purple passion fruit seeds (*Passiflora edulis* f. *edulis* Sims) as a promising source of skin anti-aging agents: Enzymatic, antioxidant and multi-level computational studies

Andres Yepes [a], Daniel Ochoa-Bautista [b,*], Walter Murillo-Arango [b], Jorge Quintero-Saumeth [c], Karent Bravo [d], Edison Osorio [d]

[a] *Grupo de Química de Plantas Colombianas, Instituto de Química, Facultad de Ciencias Exactas y Naturales, Universidad de Antioquia, UdeA, Calle 70 No. 52-21, Medellin, Colombia*
[b] *Grupo de Investigación en Productos Naturales (GIPRONUT), Departamento de Química, Facultad de Ciencias, Universidad del Tolima, Ibagué, Colombia*
[c] *Universidad de Pamplona, Facultad de Ciencias Básicas, Km 1 Vía Bucaramanga Ciudad Universitaria, Pamplona, Colombia*
[d] *Grupo de investigación en Sustancias Bioactivas, Facultad De Ciencias farmacéuticas y Alimentarias, Universidad de Antioquia, Calle 70 No. 52-21, Medellín, Colombia*

Received 25 August 2020; accepted 5 November 2020
Available online 16 November 2020

KEYWORDS

Passiflora edulis;
Enzymatic assays;
Antioxidants properties;
Anti-aging;
Molecular modeling

Abstract This study aimed to assess the anti-aging potential of the ethanol extract of *Passiflora edulis* f. *edulis* Sims seeds, through *in vitro* determination of antioxidant activity and inhibition assays of some enzymes related to skin aging. Furthermore, using *in silico* methods (docking and molecular dynamics), were established the affinity of the majority compounds of the extract on the target enzymes, ending with the prediction of drug-likeness properties. The extract showed a high total phenolic content, represented mainly by flavonoids and phenolic acids, as well as a considerable antioxidant potential measured through the DPPH, FRAP and ORAC methods. In the inhibition assays of the enzymes collagenase, elastase and tyrosinase, IC_{50} values presented were optimal. Docking studies demonstrated marked binding ability of the extract constituients (specially, fisetin, galangin and *S*-eriodictyol) to the Collagenase and Tyrosinase. Molecular dynamics validated the stability and rationality of these molecular docking studies, MM/PBSA calculations provide strong evidence for both their specific heavy binding and how enzyme-ligand complex sta-

* Corresponding author.
E-mail addresses: andresf.yepes@udea.edu.co (A. Yepes), drochoa@ut.edu.co (D. Ochoa-Bautista), wmurillo@ut.edu.co (W. Murillo-Arango), jorge.quintero@unipamplona.edu.co (J. Quintero-Saumeth), karen.bravo@udea.edu.co (K. Bravo), edison.osorio@udea.edu.co (E. Osorio).
Peer review under responsibility of King Saud University.

Production and hosting by Elsevier

https://doi.org/10.1016/j.arabjc.2020.11.011

bilized inside the catalytic domain, and drug-likeness studies showed suitable dermato-pharmacokinetics indices for most of components of extract. Findings from this study suggest that ethanol extract of *P. edulis* has a great potential as an anti-aging agent.

1. Introduction

The skin is the largest organ in the human body, accounting for about 10–15% of the body weight (Jabłońska-Trypuć et al., 2018), and is the first barrier between human body and extrinsic environment (Blume-Peytavi et al., 2016). Skin is divided into three layers: the epidermis, the dermis and subcutaneous tissue (Rittié and Fisher, 2002). The pigment producing melanocytes are scattered in the basal layer of epidermis, which determine the color of the skin and have a photoprotective function (Arda et al., 2014). The extracellular matrix (ECM) is the largest component of the dermis and provides a structural framework essential for the growth and elasticity of the skin, and it is composed mainly by matrix metalloproteins such as collagen, elastine and fibronectin, produced by fibroblasts (Bravo et al., 2016). Collagen is the primary structural component of the dermis, and is responsible for conferring strength and support to human skin (Baumann, 2007). Elastin is a protein that is present in several connective tissues and confers a unique physiological elasticity to the skin (Baumann, 2007; Halper and Kjaer, 2014).

Photoageing of skin is caused by overexposure to UV radiations, which increases the production of reactive oxygen species (ROS) (Rittié and Fisher, 2002), causing lipid peroxidation, DNA damage, and proteins alterations. Moreover, ROS can also contribute to skin ageing by direct activation of enzymes responsible for the cleavage of extracellular matrix (ECM) components (Mukherjee et al., 2011; Rittié and Fisher, 2002), as well as accelerate skin pigmentation by its action on keratinocytes, adjacent to melanocytes, to induce melanogenesis by increasing the amounts of the melanogenic factors tyrosinase and tyrosinase-related protein 1 (TRP 1) (Sasaki et al., 2000).

Skin aging is a complex mechanism characterized by a loss of skin elasticity and strength as well as the development of pigmentation disorders (Bravo et al., 2017; Greenwald et al., 2016). Moreover, hyperpigmentation, deterioration of collagen and elastin fibers resulting in wrinkles, laxity, skin dryness, poor wound healing (Swalwell et al., 2012) has been attributed to up-regulation of tyrosinase, collagenase and elastase enzymes, respectively (Koo et al., 2008; Wiegand et al., 2017). Although there are several synthetic skincare products containing ingredients active against skin aging, they can produce adverse reactions such as allergic contact dermatitis, irritant contact dermatitis, phototoxic and photoallergic reactions (Mukherjee et al., 2011).

The most popular *Passiflora* edible species around the world is 'yellow passion fruit' (*Passiflora edulis* var. flavicarpa Degenerer), however "gulupa" (Common denomination in Colombia) or "purple passion fruit" (*Passiflora edulis* f. *edulis* Sims), have a great commercial importance as well (Corrêa et al., 2016). The passion fruit seeds waste has been tapped for oil manufacturing (Pereira et al., 2019) but the residual cake remains underutilized. However, this is a valuable source of phenolic compounds for cosmetic applications (Carciochi et al., 2017; Oliveira et al., 2016). Among several of its functions, polyphenols act against harms caused by the ultraviolet (UV) and can act as radical scavengers in biological systems, and for this reason, these may be potentially useful for human skin photo-protection. In general, the relationship between the antioxidant capacity and the presence of phenolic compounds, and its subsequent benefits that can be harnessed when incorporated into cosmetic products for skin protection and anti-aging, is highly relevant. Generally, flavonols, flavones, stilbenoids, lignans, phenolic acids, and other phenolic compounds present in different plant matrices have been associated with the protective effects, and the inhibition of aging-related enzymes (Corrêa et al., 2018; Vera et al., 2019). Therefore, phenolic compounds in *Passiflora* species have a remarkable interest in this research area.

In the case of "gulupa" or "purple passion fruit", to date, there is no enough information available about the potential phenolic compounds of its seeds and a respective evaluation as an anti-aging agent. Thus, this research investigated for the first time the anti-aging properties of the ethanol extract from *Passiflora edulis* seeds against some enzymes related to the skin aging process, using *in vitro* enzymatic assays in combination with a multi-level computational strategy that including: 1) the entrance mechanism of some of the main phenolic compounds into the catalytic site, providing valuable insight into our experimental findings; and 2) the calculation of key cosmeceutical pharmacokinetic indices resulting from the previous parts of the protocol. In this perspective, *P. edulis* by itself to be an interesting plant for anti-aging cosmetic formulations.

2. Materials and methods

2.1. Plant material preparation and obtaining extract

Fruits of *Passiflora edulis* f. *edulis* Sims. were purchased from local market (Ibagué, Tolima, Colombia). The seeds were manually separated from the fruit, washed to remove pulp and juice (Milli-Q water), and placed in a drying oven (Memmert, Germany) (60° C, 24 h). Then, were crushed using liquid nitrogen and a mill (Black & Decker, USA), deposited in vials with an inert atmosphere (nitrogen gas) and stored at −80° C for subsequent extractions. To obtain the ethanol extract (EA), an ultrasonic-assisted maceration process was carried out, using ethanol (96%) acidified with HCl (1%) as the extraction solvent (Seed Ratio–solvent, 1:10). The extract obtained was sonicated (40 kHz, 30 min) and mechanically stirred (24 h). The resulting supernatant was filtered (filter paper) and the solvent was evaporated by rotary evaporation (40 °C), up to total dryness. The dried extract was stored in amber recipients and

kept under the same conditions described above until used in subsequent tests.

2.2. Determination of the total polyphenol content (TPC)

The TPC of the extract was determined by the Folin-Ciocalteu method, according to the conditions described previously (Singleton, Orthofer, & Lamuela-Raventós, 1999), adapted by Bravo et al., (2015). 30 μL of extract solution prepared in distilled water was placed in each well of a 96-well microplate with 150 μL of a 1/10 dilution of Folin-Ciocalteu reagent. 3 min later, 100 μL of 75 mg/mL sodium carbonate was added. The plate was stirred for one minute using a vortex and incubated for 60 min at room temperature, protected from light. Subsequently, the absorbance was read at 760 nm in a Synergy HT multimodal microplate reader (BioTek Instruments, Inc.; Winooski, USA). The quantification was calculated using a calibration curve with a standard of gallic acid at known concentrations. Each reaction was performed in triplicate. The results are expressed as milligrams of gallic acid per gram of extract (mg GA/g).

2.3. Identification and quantification of phenolic compounds of ethanol extract

2.3.1. UPLC-MS/MS parameters

Ultra performance liquid chromatographic and mass spectrometry analysis were performed following a method previously reported (Delpino-Rius et al., 2015). UPLC analysis was carried out on a Waters ACQUITY UPLC™ system (Waters, Milford, MA, USA) consisting of an ACQUITY UPLC™ binary solvent manager and ACQUITY UPLC™ sample manager. Compounds were separated with an ACQUITY UPLC™ HSS T3 column (1.8 μm; 2.1 mm × 150 m m) (Waters, Manchester, UK) using a mobile phase consisting of solvent A, H_2O (0.1% v/v Acetic acid (HAcO)), and solvent B, ACN 100% (0.1% v/v HAcO). The flow rate was 0.550 mL/min. The linear gradient was as follows: 0–1.89 min, 1% B, (isocratic); 1.89–17.84 min, 30% B, (linear gradient); 17.84–21.39 min, 5% B, (linear gradient); 21.39–21.56 min, 1% B, (linear gradient); and 21.56–25 min, 1% B, (isocratic). Weak and strong needle solvents were H_2O (0.1% v/v HAcO) and MeOH, respectively. The injection volume was 20 μL in mode full loop, and the column was kept at 45 °C whilst the temperature in the sample manager was maintained at 10 °C.

MS analysis was carried out on a Waters ACQUITY TQD tandem quadrupole mass spectrometer (Waters, UK), following a method previously described (Delpino-Rius et al., 2015), with some modifications. The instrument was operated using an electrospray source (ESI) in positive and negative ion mode. The ESI parameters were as follows: capillary voltages of 3 kV and 2.5 kV in positive and negative mode, respectively; the source at 150 °C; desolvation temperature 500 °C; cone gas (nitrogen) flow 1000 L/h; and desolvation gas flow 800 L/h. Flow injections of each standard were used to optimize the cone voltage and Multiple Reaction Monitoring (MRM) parameters. Collision-induced dissociation was achieved using argon at a flow rate of 0.15 mL/min in the collision cell. MassLynx 4.1 software (Waters, USA) was used for data acquisition. Identification and quantification of phenolic compounds were performed employing the MRM transitions of the analytes in the retention times registered by the commercial standards of each phenolic compound (see suplementary data). All stock standard solutions of phenolic compounds were prepared in MeOH and stored at 80 °C. Working solutions were prepared from stock solutions by sampling an aliquot and diluting it with the injection solvent H_2O (0.1% HAcO).

2.4. Antioxidant activity

2.4.1. DPPH method

The stabilization of the 2,2-diphenyl-1-picrylhydrazyl (DPPH) free radical by the ethanol extract components was assessed applying a method previously described (Brand-Williams et al., 1995), with some modifications. Firstly, 200 μL of an ethanol solution of the radical (0.5 mM) were added to each well in a 96-well plate. Then, 50 μL of the extract (Ethanol solution) were mixed with the radical (1:4 sample:radical) using concentrations between 9.77 and 625 μg/mL. The reaction was incubated (30 min at room temperature and darkness), and its absorbance was read (517 nm) in a 96-well plate UV–vis reader (Multiskan® GO Thermo Scientific, USA). Each reaction was performed in triplicate. The potential of the extract to stabilize the DPPH radical was determined by the following equation :

$$DPPH\ \ Stabilization\% = \left(\frac{Control\ \ absorbance - Extract\ \ absorbance}{Control\ \ Absorbance}\right) \times 100 \quad (1)$$

Control absorbance refers to the absorbance of the ethanolic extract without the DPPH radical measured a 517 nm. The stabilization concentration 50 (SC_{50}) for the seed ethanol extract was determined using the concentrations described above.

2.4.2. Ferric reducing antioxidant power (FRAP)

Measurement of the reducing power of the extract was carried out using a previously described procedure (Jiménez et al., 2015) with some modifications (Duque et al., 2017). The FRAP working solution contained acetate buffer (300 mM, pH 3.6), TPTZ (2,4,6-tripyridyl-s- triazine) (10 mM) in HCl solution (40 mM) and $FeCl_3{\cdot}6H_2O$ (20 mM) at a 10:1:1 ratio to provide the reducing solution, and Trolox was used as a standard. First, 10 μL of sample (Dimethyl sulfoxide solution of ethanol extract or Trolox standard) was added to each well in a 96-well plate, mixed with 250 μL FRAP working solution, and incubated at 37 °C for 10 min in the dark. Each reaction was performed in triplicate. The absorbance was measured at 593 nm using a Synergy HT Multi-mode-microplate reader. The results were expressed as μmol Trolox Equivalent per gram of extract (μmol TE/g).

2.4.3. Oxygen radical absorbance capacity (ORAC) assay:

The hydrophilic ORAC assay was performed using a previously described procedure (Bravo et al., 2015), with some modifications (Bravo et al., 2016). AAPH (2,2′-Azobis(2-amidinopropane) dihydrochloride) was used as a peroxyl radical generator, and Trolox was used as a standard. Moreover, fluorescein was used as the fluorescent probe. Fluorescein, AAPH and the samples were prepared in phosphate buffer (75 mM, pH 7.4). First, 25 μL of sample (Dimethyl sulfoxide solution

of ethanol extract or Trolox standard) was mixed with 150 µL of fluorescein (1 µM) and pre-incubated at 37°C for 30 min before the addition of 25 µL of AAPH solution (200 mM). Each reaction was performed in triplicate. The fluorescence at an excitation wavelength of 485 nm and an emission wavelength of 520 nm was measured every 2 min for 120 min using a Synergy HT Multi-Mode Microplate Reader (BioTek Instruments, Inc.; Winooski, USA). The relative ORAC values were calculated using the differences of areas under the decay curves and were expressed as µmol TE/g of extract.

2.5. Antiage activity

2.5.1. Anti-collagenase activity

The effect on the collagenase enzyme was measured using the EnzCheck® Gelatinase/Collagenase Assay Kit (Molecular Probes Inc, USA), following a procedure previously described (Bravo et al., 2016). Collagen type 1 from bovine skin was used as substrate. Briefly, 80 µL of extract solution prepared in Tris-HCl buffer (0.05 M, pH 7.6), or 80 µL of this buffer (Control), were added to each well in a 96-well plate along with 20 µL of the 125 µg/mL DQ™- collagen substrate. Subsequently, 100 µL of the 1 U/mL active enzyme was added and the fluorescence intensity was measured every 45 min for 415 min (λ Excitation = 285 nm, λ Emission = 515 nm), using a Synergy HT multimodal microplate reader (BioTek Instruments, Inc, USA). To determine the inhibitory potential of the EA, the slope of the linear line (20 min) of the fluorescence vs. time graph was obtained and compared with the slope obtained for the control. The percent inhibition of collagenase reaction was calculated as follows:

$$Inhibition\% = \frac{M_{Control} - M_{Sample}}{M_{Control}} \times 100$$

where $M_{Control}$ and M_{Sample} are the slopes of the graph fluorescence vs time of the control and sample, respectively. The IC_{50} of the extract was measured between 3.125 and 50 µg/mL. Oleanolic acid was used as a reference inhibitor. Each reaction was performed in triplicate.

2.5.2. Anti-elastase activity

The inhibition of the elastase enzyme was measured using the EnzChek® Elastase Assay Kit from Molecular Probes Inc., following a procedure previously described (Bravo et al., 2016). Aliquots of 50 µL of extract solutions (Dimehtyl sulfoxide solution of ethanol extract) or buffer (control) were mixed with 50 µL of 125 µg/mL DQ™- elastine substrate and 100 µL of 0.5 U/mL enzyme solution. The fluorescence intensity was measured by a Synergy HT Multi-Mode Microplate Reader (BioTek Instruments, Inc.; Winooski, USA) for excitation at 485 nm and emission detection at 515 nm at each minute for 30 min. Percentage of elastase reaction inhibition was calculated employing the equation (2). IC_{50} of the extract was measured between 25 and 500 µg/mL. Oleanolic acid was used as a reference inhibitor. Each reaction was performed in triplicate.

2.5.3. Anti-tyrosinase activity

The anti-tyrosinase assay was carried out by a method previously described (Bravo et al., 2016). Briefly, 70 µL of sample solutions prepared in phosphate buffer (50 mM, pH 6.5) or buffer (control) were mixed with 30 µL of 333 U/mL mushroom tyrosinase and 110 µL of 2 mM L-tyrosine solution into a 96-well plate. The absorbance was measured at 480 nm each minute for 30 min. Percentage of elastase reaction inhibition was calculated employing the equation (2). IC_{50} of the extract was measured between 18.75 and 4800 µg/mL. Kojic acid was used as a reference inhibitor. Each reaction was performed in triplicate.

2.6. Cytotoxicity evaluation

Human leukocytes from healthy donors obtained by Ficoll gradient (Alberto Checa Rojas, 2018) were used. Briefly, 5 mL of anticoagulated whole blood was taken in a 15 mL falcon tube previously loaded with 5 mL of Phosphate-Buffered Saline (PBS) (pH 7.4 sterile), and the mixture was homogenized by immersion. In another falcon tube, 3 mL of Ficoll-1077 was dispensed. Then 10 mL of the whole blood and PBS mixture were taken and carefully placed on the surface of the Ficoll-1077 without disturbing the interface, slowly draining the mixture through the wall of the inclined tube. To finish the cell layers formed, the tubes were carefully centrifuged at 300 rpm for 20 min. Then, the tubes are removed avoiding disturbance of the formed layers. Dry ethanolic extract was dissolved in DMSO to prepare different dilutions to take into account a 1:5 ratio between the EA extract and resazurin, to complete concentrations of extract between 1000 and 4000 µg/mL, ensuring a maximum DMSO concentration of 1%. This was prepared as a metabolic indicator at 440 uM to obtain a final concentration of 44 uM in the 96-well plates. The determination of cell viability was measured by taking 50 uL of the previously isolated leukocyte solution, adding 50 uL of the different concentrations of the prepared extracts and 10 uL of resazurin, and incubating for 30 min at 37 °C. The absorbance was read in a spectrophotometer at 570 nm and 603 nm (Czekanska, 2011). Viability percentage was calculated through the following equation:

$$Viability\% = \frac{M \times 100}{C} \quad (3)$$

were: M = absorbance of the cells treated with the extract, and C = absorbance of the cells not treated with the extract.

2.7. Multi-level computational studies

2.7.1. Protein structure and setup

Finding the bioactivity on anti-aging targets, molecular docking studies were performed into the catalytic domain of the 3D structures of human fibroblast collagenase (PDB entry code 1CGL), porcine pancreatic elastase (PDB entry code 1QNJ), and tyrosinase (PDB entry code 2Y9X) respectively (Ismaya et al., 2011; Lovejoy et al., 1994; Würtele et al., 2000). The information about the experimental resolution of each protein were obtained from the Protein Data Bank. Discovery Studio (DS) Visualizer 2.5 was used to edit the protein structure to remove water molecules together with bound ligands, excluding copper and Nickel (II) ions. For docking studies, the structure of the selected protein was parameterized using AutoDock Tools (Trott and Olson, 2009). In general, hydrogens were added to polar side chains to facilitate the formation of hydrogen bonds, and Gasteiger partial charges were calculated. AutoDock saved the prepared protein file in PDBQT format.

2.7.2. Ligand dataset preparation and optimization

Ligands used in this study were the major components found in *P. edulis* seeds extract and oleanolic acid, kojic acid and tropolone, three well-known competitive inhibitors currently used as the positive control. Thus, the 2D structures of the eight *P. edulis* constituents and three standards were obtained as mol2 files from the ZINC database (Irwin et al., 2012). The resultant compounds were submitted to MarvinSketch 8.3 ("Marvin - ChemAxon," 2007) to correct the protonation states of the molecules at pH 7.4 and its structures parameterized using AutodockTools to add full hydrogens to the ligands, to assign rotatable bonds, to compute Gasteiger charges and saving the resulting structure in the required format for use with AutoDock. All possible flexible torsions of the ligand molecules were defined using AUTOTORS in AutoDockTools (Morris et al., 2009, 1998) to promote the calculated binding with the selected anti-aging targets.

2.7.3. Docking and posterior analysis

Docking simulations were performed with AutoDock 5.6 using the Lamarkian genetic algorithm and default procedures for docking a flexible ligand to a rigid protein were followed. The docking analysis was carried out into the reported catalytic site of each protein. Once a potential binding site was identified, docking of ligands to this site was carried out to determine the most probable and most energetically favorable binding conformations. For this purpose, more rigorous docking simulations involving a smaller search space limited to the identified binding site, Autodock Vina (Trott and Olson, 2009) was used. The exhaustiveness (internal number of repetitions) was 20 for each protein-compound pair. The active site was surrounded by a docking grid of 40 $Å^3$ with a grid spacing of 0.375 Å. Docking solutions obtained from all molecules analyzed were ranked by the affinity scores given by AutoDock Vina based on the free energy binding theory (more negative score indicates higher affinity). Resulting structures and some of the docked conformations were graphically inspected to check the interactions using DS visualizer or The PyMOL Molecular Graphics System, Version 2.0 Schrödinger, LLC.

2.7.4. Molecular dynamics and binding energy-MM-PBSA studies

In order to verify the molecular interaction stability of protein–ligand complexes, molecular dynamics (MD) simulations were carried out by using the Gromacs program (Abraham et al., 2015) considering the most docking-active components (fisetin for collagenase and galangin for Tyrosinase) and the best pose of each molecule. Force field parameters for protein and ligands were derived independently. For both collagenase (PDB ID: 1CGL) and tyrosinase (PDB ID: 2Y9X) proteins, the amber03 force field was select and assigned by using the pdb2gmx tool of the Gromacs program packages, meanwhile ligand force field parameters were prepared with the generalized AMBER force field (GAFF) using the molecular geometries previously optimized in gas phase using the HF/6–31* level of theory, (Ditchfield et al., 1971; Frisch et al., 1984; Hariharan and Pople, 1973; Hehre et al., 1972; Roothaan, 1951) with the Gamess-US program (Schmidt et al., 1993). In addition, each ligand was verified as a minimum through a harmonic vibrational normal mode analysis. Atomic charges were obtained with the Merz-Kollman scheme (Singh and Kollman, 1984) by fitting a restricted electrostatic potential (RESP) model (Bravo et al., 2017) by the Gamess-US program, and the output file was used into the resp subprogram of the AmberTools program package (Bayly et al., 1993). Assignment of GAFF force field parameters was carried out by the Antechamber program (Cornell et al., 1995) and the required input files for molecular dynamics simulations were prepared using the ACPYPE python interface (Wang et al., 2006). Protein and protein–ligand complexes were solvated in a rectangular box of TIP3P waters and chloride (Cl^-) or sodium (Na^+) ions were added to the system by random replacement of water molecules until neutralization of total charge. In order to remove spurious contact, molecular geometries were optimized with the steepest descent algorithm with 100,000 steps, protein backbones atoms were constrained with a force constant of 1000 kJ mol^{-1}. Then, the MD simulations was allowed to run for 1000 ps in the NpT ensemble. Additionally, 40 ns in the NpT ensemble were calculated for the production stage. All simulations were carried out under periodic boundary conditions. A 12 Å cutoff distance was used to calculate non-bonded interactions. Electrostatic interactions were treated with the Ewald particle mesh (PME) method (Darden et al., 1993; Sousa Da Silva and Vranken, 2012); while van der Waals interactions were introduced by using the cut-off scheme. Finally, the V-rescale thermostat at 300 K with a coupling constant of 1.0 ps was used and the pressure was kept constant at 1 atm using the Parinello-Rahman barostat (Essmann et al., 1995; Parrinello and Rahman, 1981) with a coupling constant of 2.0 ps and a compressibility factor of 4.5x10-5 bar-1. All covalent bonds were constrained using the LINCS algorithm and the contact list was updated every 40 fs. The binding free energy was analyzed using the molecular mechanics Poisson − Boltzmann surface area (MM/PBSA) method (Kollman et al., 2000) implemented in Gromacs program. For MM-PBSA calculations, the g_mmpbsa software (Kumari et al., 2014) was used for electrostatic interactions, van der Waals interactions, polar solvation energy, and non-polar solvation energy calculations. The binding free energy was calculated using the last 35 ns of trajectories from the production stage MD simulations, e.g. 3501 snapshots. The SASA model was used for non-polar contributions with a surface tension of 0.0226778 (kJ/mol2) and a probe radius of 1.4 Å. Ionic strength of 0.150 M NaCl with radii of 0.95 and 1.81 Å for sodium and chloride ions respectively was used for all polar calculations. In addition, dielectric constants of 6, 80 and 1 were used for the protein, water, and vacuum respectively. To calculate the average binding free energy over the previously selected snapshots, a bootstrap analysis was performed.

2.7.5. Prediction of drug-likeness properties for the most docking promissory compounds

To find out the cosmeceuticals properties for the majoritarian components in *P. edulis* seeds, the physicochemical descriptors were determined using open-source cheminformatics toolkits such us Molinspiration software (for: MW, H-bond donors, H-bond acceptors descriptors) and ALOGPS 2.1 algorithm from the Virtual Computational Chemistry Laboratory (for: LogPo/w and aqueous solubility LogSw descriptors). These parameters enabling rapid screening of good or bad skin penetrants for topical use and can be used to predict violations to transdermal rule of five, which good penetrants had

MW $\leq$ 300, log Sw $>$ $-$ 2.3, H-bond donors $\leq$ 5, H-bond acceptors $<$ 5, LogPo/w $<$ 2.6 (Choy and Prausnitz, 2011; Magnusson et al., 2004a)

Furthermore, to obtain the information of kinetics of adsorption and distribution required for skin permeability, four important dermatopharmacokinetic parameters were predicted for the mayor compounds: the skin permeation coefficient of chemical in the stratum corneum ($LogK_p$) was calculated using the Potts model (Bunge and Cleek, 1995) (Guy and Potts, 1993; Potts and Guy, 1992) according to the equation [$LogP_{ab} = -2.74 + 0.71.Log\ P_{o/w} - 0.0061.MW$], the effective diffusion coefficient in the human dermis (D_{de}) was calculated by the Bunge model using the equation [$D_{de} = (7.1x10^{-6}/MW^{0.5})$] (Bunge and Cleek, 1995), the most important parameter in determining the maximal dermal flux, toxic, or systemic effect J_{max} was predicted using the equation [$Log\ J_{max} = -3.90 - 0.0190.MW$], which good penetrants had values $>$ 2.52 (Magnusson et al., 2004b, 2004a) and the partition coefficient between human stratum corneum lipids and water was predicted using the Hui model by equation [$LogK_{sc/w} = 0.078.(LogP)^2 + 0.868.LogMW - 2.04$] (Hui et al., 1995). These important parameters that define penetration, absorption, permeation, movement, partitioning and diffusion, has been applied to support transdermal delivery of potential drugs and skincare actives as well as integrated risk assessment (Chen et al., 2015; Milewski and Stinchcomb, 2012; Schoellhammer et al., 2014; Zhang et al., 2009).

3. Results and discussion

3.1. Total phenolic content, antioxidant and anti-aging activity

In this research, antioxidant activity and inhibitory activity against skin aging-related enzymes were determined. The antioxidant capacity of the extract determined by different methodologies is displayed in Table 1. There it is shown that the total high phenolic content (0.32 $\pm$ 0.04 g GA/g extract), is comparable to that reported by (Oliveira et al., 2016), who evidenced a content of 0.39 $\pm$ 0.1 g GA/g extract of defatted passion fruit seeds.

Additionally in the same study, the extract evaluated is capable of acting as a prebiotic with antioxidant activity when analyzed through ORAC and DPPH. Considering the results of previous research, the TPC is responsible for the remarkable antioxidant activity presented by the ethanol extract of the gulupa seed (Table 2) evaluated by the methodologies of DPPH, FRAC, and ORAC. In regards to these values, it is important to mention that there is a diversity of extraction protocols that make it difficult to compare the results, and even some authors have shown that the concentration of phenols can be increased when different variables associated with the extraction process are optimized (de Santana et al., 2017). For Example Passion fruit seed extract obtained from juice production residue by methanolic wáter reflux and further liquid–liquid partition, showed differential action depending on fraction polarity, being the most potent antioxidant the EtOAc fraction (IC_{50} DPPH = 2.7 $\pm$ 0.2). This fraction exhibited the most ferric reducing power as well (EC 1 mM $FeSO_4$ = 2,813. 9 $\pm$ 11.6) and tyrosinase inhibitory effect (39.9 $\pm$ 0.0% at 1 mg/mL), besides sun protection factor of the EtOAc extract was comparable to ferulic acid (Lourith and Kanlayavattanakul, 2013). In the same vein, they also studied the ethanol extract of *P. edulis* seeds, state that the processing residue of passion fruit juice (seed) is a source of functional compounds, and the antioxidant fraction works as a sunscreen with effective protection against UV rays, as well as a skin-whitening agent (Lourith et al., 2017), while other studies have been reported values of 41,67 $\pm$ 0,30 µmol ET/g in ORAC antioxidant activity for a methanol extract of *P. edulis* seed (Vagula et al., 2019).

Regarding the inhibition of collagenase, elastase and tyrosinase enzymes, the IC_{50} values were 28.29, 32.92 and 141.30 µg/ml respectively. Previous studies on seeds and peels of *P. edulis* determined that 70% ethanol extracts of peel and seed had IC_{50} values of 122.70 $\pm$ 6.35 and 67.35 µg/ml $\pm$ 6.58, as regards anti hyaluronidase activity. Also, IC_{50} value of elastase inhibitor of peel and seed extract was 62.82 $\pm$ 1.50 µg/mL and 41.06 $\pm$ 0.31 µg/mL respectively. With these findings, it can be suggested that the seeds and peel may have the potential as a source of anti-aging ingredients (Hartanto et al., 2019; Vera et al., 2019). Extracts and fractions of *P. tarminiana* fruits showed high polyphenol content (620 mg EAG /g) and antioxidant activity, as measured by ORAC (4097 µmol ET/g) and ABTS (2992 µmol ET/g) assays. The aqueous fraction drastically inhibited the collagenase enzyme (IC_{50} 0.43 µg/mL). The extract and fractions presented photoprotective effects by reducing UVB-induced MMP-1 production, increasing UVB-inhibited procollagen production, and decreasing ROS (Bravo et al., 2017). The results found for the ethanol extract of the gulupa seeds presented in our study are following what has been previously reported for the seeds of different passion flower species, and especially as other authors have shown that seed extracts may be a source that can be used in the formulation of green cosmetic products with anti-age and anti-wrinkle properties, thereby generating the valuation of this agro-industrial by-product.

3.2. Phenolic composition of ethanol extract

Table 2 shows the chemical composition of the EA extract. Two main groups of phenolic compounds were observed: Flavonoids and Phenolic acids. The first group is highlighted as the largest group of compounds analyzed (897,07 ng/mg of extract), being Genistein the most abundant compound (690,386 ng/mg of extract). On the other hand, Phenolic acids presented a considerable abundance (437,476 ng/mg of extract) in the ethanol extract composition. In this group, Protocatechuic acid was the most abundant compound (181,235 ng/mg of extract).

Due to the limited reports about the chemical composition of the seeds of *Passiflora edulis* f. *edulis* Sims., most of the references to get useful information regarding this and establish comparisons between studies as well, are taken from other *Passiflora* species reports. Some of those studies have evaluated the phenolic content of extracts obtained from the seeds of several *Passiflora* species by using solvents of different polarities, especially passion fruit (*Passiflora edulis* var. *flavicarpa*), species that is object of the major part of those studies.

In this regard, they have been able to identify considerable amounts of chlorogenic and rosmarinic acids, together with quercetin, in the ethyl acetate fraction, while reasonable amounts of kojic and gallic acids were found in the aqueous

Table 1 Antioxidant and inhibitory capacity on different enzymes associated with cutaneous aging processes of ethanol extract (EA) of *P. edulis* seeds.

	Antioxidant evaluation				Inhibitory capacity IC_{50} (μg/ml)		
	TPC (gAG/g extract)	DPPH• (SC_{50})	FRAP (μmol TE/g extract)	ORAC (μmol TE/g extract)	Anti-colagenase	Anti-elastase	Anti-Tyrosinase
EA ethanol extract	0.32 ± 0.04	132.6	14.2 ± 0.4	18.3 ± 0.5	28.29	32.2	141.3
Oleanolic acid[a]	–	–	–	–	37.18	–	–
Oleanolic acid[b]	–	–	–	–	–	327.34	–
Kojic acid[c]	–	–	–	–	–	–	0.481

Table 2 Phenolic composition of the ethanol extract (EA) of Passiflora edulis seeds.

Compound	EA (μg/mg)
Salicylic acid	0.0858
Protocatechuic acid	0.1812
p-coumaric acid	0.0150
Vanillic acid	0.0901
Galic acid	0.0104
Caffeic acid	0.0485
Ferulic acid	0.0026
Syringic acid	0.0014
Daidzein	0.00001
Galangin	0.07424
Genistein	0.6903
Fisetin	0.0250
Luteolin	0.0043
Kaempferol	0.0078
Eriodictyol	0.0680
Catechin	NQ
Epicatechin	NQ
Quercetin	NQ
Taxifoline	0.0019
Clorogenic acid	0.0022
Luteolin 7-O-glucoside	0.00601
Quercetin-O-glucopyranoside	0.0052
Naringin dihydrochalcone	0.0065
Vicenine II	0.00001
Theaflavin digalate	0.0067
Total flavonoids	0.8970
Total phenolic acids	0.4375

seed fraction (Lourith and Kanlayavattanakul, 2013). In the same study, the presence of scirpusin B and stilbene piceatannol was reported, simply and dimerically in passion fruit seeds, and a previous study the compound was reported as the majority phenol in gulupa seeds (Matsui et al., 2010).

The results of the phenolic composition of the gulupa seeds reported in this work are consistent with the kind of phenolic present in seed, however, some differences can be observed in the types of compounds reported, possibly due to the variable extraction conditions, and the use of analytical identification techniques as well (Gadioli et al., 2018). Phenolic compounds from hydroalcoholic extracts of the seeds presented high content of TPC, and mainly flavonoid type compounds, being able to identify quercitrin, coumaric acid, epicatechin, chlorogenic acid and rutin (González et al., 2019).

3.3. In vitro blood cell viability profiling

To optimize the development of novel topical formulations for the treatment of skin disorders, preclinical toxicity testing is a very important step. For this purpose, OECD (Guidelines for Testing of Chemicals) recommends sequential testing strategies for dermal toxicity measures during the development of topical delivery systems (www.oecd.org). Among them, dermal toxicity on human keratinocyte and fibroblast cultures correspond to the current pre-clinical evaluation of novel cosmeceutical products (Ponec et al., 1990). However, topically applied therapeutics that permeate through the stratum corneum, could entry into the systemic circulation via the dermal microcirculation and adverse effects may occur (Abraham, 2014; Alikhan and Maibach, 2011). Hence, in addition to dermal toxicity, transdermal formulations need to be early evaluated against blood cells in order to ensure less harmful. In this work, *in vitro* studies using human leukocytes model were carried out in order to evaluate potential toxicity a systemic level. The results showed that the ethanol seeds extract did not generate toxic effects at the different evaluated concentrations, and on the contrary, cell viability was observed, slightly higher than that of the control treatment (values not shown). This approach allowed us to study how components of the extract could be behavior after entering through the blood vessel, to aim potentially mitigate blood adverse reaction, however more robust testing including *in vitro* test to determine mutagenicity, carcinogenicity, and toxicity for reproduction would be necessary for the future.

3.4. Multi-level computational results

Integrating virtual docking, molecular dynamics (MD) and MM-PBSA approaches for measure the effectiveness of the main components of ethanol extract of gulupa seeds against aging-related enzymes were performed. Our protocol allowed us to predict the inhibitory capacity of the main constituents of ethanol extract of *P. edulis* against X-ray crystal structures of the age-associated enzymes retrieved from RCSB Protein Data Bank as follow: fibroblast collagenase, native porcine pancreatic elastase, and mushroom tyrosinase, PDB Codes 1CGL (Lovejoy et al., 1994), 1QNJ (Würtele et al., 2000)

and 2Y9X (Ismaya et al., 2011), respectively. This study was performed to identify which components of the ethanol extract from *P. edulis* could act against aging-associated enzymes. Also, molecular dynamics simulations were carried out to investigate the stability of the selected components into the catalytic domain of these enzymes and MM-PBSA method was used to estimate the different contributions to the binding free energy. Furthermore, we explore drug-likeness properties for the most promising compounds resulting after docking runs.

Processes of skin aging are associated with the breakdown of elastin and collagen by the elastase and collagenase enzymes. The protein elastin is responsible for skin elasticity while collagen is responsible for the elasticity and strength of the skin maintaining its flexibility. Hence, inhibiting the function of elastase and collagenase enzymes suggested as key factors to prevent not only the loss of skin elasticity but also the progress of aging-induced by photoaging (Wittenauer et al., 2015). On other hand, tyrosinase is a multifunctional copper-containing polyphenol oxidase, know to affect the rate-limiting in melanin biosynthesis. Tyrosinase participates in many types of skin disorders, including hyperpigmentation, melasma, and lentigo in mammals and mainly, skin cancer (Rao et al., 2013). Thus, the regulation of melanin synthesis by inhibitors of tyrosinase could help prevent serious disease related to skin hyperpigmentation and used them as cosmetics materials as skin whitening agents. Computational docking refers to physical three-dimensional structural interactions that provide a means to predict and assess interactions between ligands (small molecules, proteins, peptides, etc.) and proteins (typically, proteins, DNA, RNA, etc.) (Horst et al., 2012). Docking methods are evaluated by predicting the correct pose/binding mode or by measuring predicted binding affinities

Considering the importance of aging-related proteins and in order to propose a molecular level explanation based on the experimental results against elastase, collagenase, and tyrosinase inhibition, herein we used docking as a reasonable approach to investigate the molecular affinity of the mayor constituents containing in ethanol extract of *P. edulis* (genistein, protocatechuic acid, vanillic acid, salicylic acid, galangin, *S*-eriodictyol, caffeic acid and fisetin) against the three-dimensional structure of three aging-related enzymes: collagenase (PDB: 1CGL), elastase (PDB: 1QNJ) and tyrosinase (PDB: 2Y9X), respectively. The most important pocket for the inhibitory activity for collagenase is the binding domain located around the putative zinc-binding and comprising a histidine catalytic triad: HIS218, HIS222, HIS228, hence these zinc-binding residues should be considered for designing an inhibitor for collagenase. For elastase are situated around the catalytic triad comprising HIS57, ASP102 and SER195. In the case of tyrosinase the catalytic segment is positioned around the binuclear copper-binding site in the deoxy-state, which both three histidine residues coordinate each copper ion as follow: Cu-A (HIS85, HIS 94, HIS61) and Cu-B (HIS296, HIS259, HIS263) and water bridging the two copper ions, which are critical for both catalytic activities of tyrosinase. (Farrokhnia and Mahnam, 2017; Ismaya et al., 2011; Sivamani et al., 2012). Fig. 1 illustrates the cleavage site of metalloproteins collagenase and tyrosinase selected in this computational study, which show critical interactions between metal ions with histidine residues essential for its catalytic activities.

In general, the major components from ethanol extract of *P. edulis* displayed good binding affinities for the selected pockets, most of them higher than current inhibitors. The most favored docking poses for the complexes between key aging enzymes and these compounds and current inhibitors (used as references) are listed in Table 3. Notably, after docking runs the main compounds studied showed appeared to have the highest affinity on collagenase protein. Amongst them, fisetin (-8.7 kcal.mol^{-1}), *S*-eriodictyol (-8.4 kcal.mol^{-1}) and galangin (-8.0 kcal.mol^{-1}) displayed marked association to crystallized fibroblast collagenase (PDB: 1CGL) in comparison with the current inhibitor oleanolic acid, which have a docking score of −8.1 kcal.mol^{-1}. This result is consequent by our enzyme activity measurements, in which EA showed most effectiveness against collagenase enzyme (IC_{50} value of 28.29 μg/mL) compared with those elastase and tyrosinase. Our results are according to the findings in the literature, which integrative *in vitro*, *in vivo* and *in silico* studies showed potent skin protective effects for galangin, *S*-eriodictyol, and fisetin (Grynkiewicz and Demchuk, 2019; Polito et al., 2012; Wen et al., 2020).

Interestingly, when the main phenolic components of ethanol extract from *P. edulis* were docked against the 3D-structure of tyrosinase showed higher binding affinities than those current inhibitors (kojic acid −5.6 kcal.mol^{-1} and tropolone −5.8 kcal.mol^{-1}), specially galangine with a docking score of −8.0 kcal.mol^{-1}, followed by genistein (−7.6 kcal.mol^{-1}) and *S*-eriodictyol (−7.3 kcal.mol^{-1}). This result is correlated with previous reports which notable *in vitro* and *in vivo* inhibitory effects for these compounds on mushroom tyrosinase has been determinate (Chung et al., 2018; Jiménez-Atiénzar et al., 2005; Yang et al., 2008). Due to the remarkable presence of these compounds in ethanol extract of *P. edulis*, we believe based on our enzymatic and *in silico* studies at least point at *P. edulis* as whole as an interesting herb for antiaging purposes in human skin by collagenase and tyrosinase inhibition and should be taken into consideration in cosmeceutical formulations. From the docking perspective, fisetin (affinity of −8.7 kcal.mol^{-1} to collagenase), *S*-eriodictyol (affinity of −8.4 kcal.mol^{-1} to collagenase), galangin (affinity of −8.0 kcal.mol^{-1} to tyrosinase) have focused special attention in the present study. Thus, we performed a rigorous exploration of the docking solutions obtained from these compounds when docked occurred against aging-related enzymes, which resulted particularly interesting by correlating the enzymatic with computational findings. Hence, based on the analysis of these different results an visual inspection, a clear behavior appears along the molecular docking that could be summarized as follows (Fig. 2):

3.4.1. Collagenase docking profile

A first analysis consisted in the simulation of the ligands galangin, *S*-eriodictyol and fisetin to the cleavage site of collagenase. Then, to compare the best binding pose each of the most docking-active components of ethanol extract of *P. edulis* with a potent collagenase inhibitor (oleanolic acid), Fig. 2A-D illustrates the most stable binding poses based on AutoDock scoring listed in Table 3 for the active compounds (those with the high binding affinity after docking) on collagenase catalytic domain.

The superposition of the inhibitor oleanolic acid (*in red*) and the best conformation obtained theoretically for selected docked compounds, showed that the most active component of the ethanol extract of *P. edulis* (obtained by docking

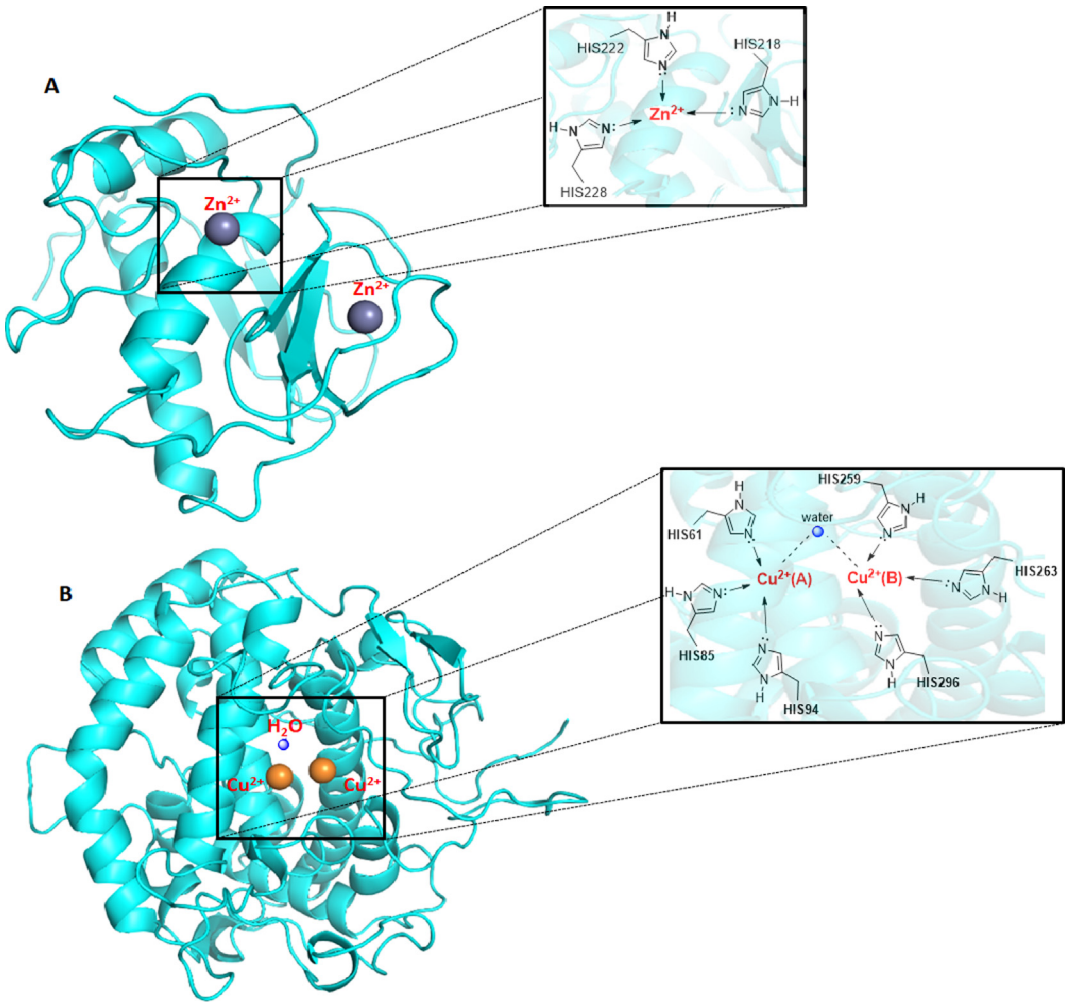

Fig. 1 (**A**) Histidine triad Chelates Zinc into the cleavage active site of collagenase. (**B**) binuclear copper-binding site chelates by six conserved histidine residues on tyrosinase enzyme.

simulation) can accommodate themselves into stable conformations occupying this catalytic binding site during docking process.

Fig. 3A-C illustrates 3D and 2D representations into the cleavage site on collagenase enzyme for the compounds which exhibited the highest docking score (galangin, *S*-eriodictyol and fisetin). We examined which interactions are involved when these compounds were docked against collagenase and how their structures affect them. In general, analysis of the docking solutions revealed at least 14 amino acids are involved in the ligand-collagenase interactions. Moreover, an inspection of the docking conformations showed that the most active molecules complexed with the human fibroblast collagenase have an interaction fingerprint involving six residues in the catalytic pocket, HIS218, VAL215, GLU219, TYR237, ASN180 and PRO238. As aforementioned, the Zn^{2+} on the collagenase enzyme is involved in the catalytic process coordinates to three residues of histidine, among them HIS218 residue plays an important role in collagenase catalytic function. Hence their participation is notable (Manzetti et al., 2003). All docked compounds showed π-π stacking contact through interaction between aryl moiety and imidazole ring on key HIS218 residue. This finding, suggesting a slowly reversible mechanism of inhibition that is aided by strong non-covalent association with the HIS218 residue through π-π contact, hence galangin (*in yellow*), *S*-eriodictyol (*in magenta*) and fisetin (*in cyan*) could be act blocking Zn^{2+} during catalysis or disrupting the noncovalent interactions when Zinc is bound to histidine or water. These findings may explain the *in vitro* effectiveness of the *P. edulis* ethanol extract against collagenase diagnosed by our enzymatic assay.

Furthermore, a rigorously bonding analysis of galangin, *S*-eriodictyol and fisetin against human collagenase revealed notable non-covalent interactions that may stabilize the binding event into collagenase active site. Thus, galangin (−8.0 kcal/mol) has π-alkyl interaction with VAL215 residue, carbon-hydrogen bond with ASN180 and several hydrophobic interactions between the molecule and the ALA182, PRO238, HIS222, HIS183, TYR240, LEU181 residues. *S*-eriodictyol (−8.4 kcal/mol) that had better affinity than to the inhibitor oleanolic acid establishing two strong hydrogen bond interactions between the 3-hydroxyl group in aryl moiety with TYR237 and ARG214 residues. In addition, three π-stacking contacts were formed between molecule with SER239,

Table 3 Best binding energy (kcal/mol) based on AutoDock scoring of the main constituents from *Passiflora edulis* into the active sites of collagenase, elastase and tyrosinase enzymes.

Compounds	*Binding energy (kcal/mol)*[a]		
	Anti-collagenase	Anti-elastase	Anti-tyrosinase
Genistein	**−7.8**	−6.9	**−7.6**
Protocatechuic acid	−6.7	−5.6	−6.0 −6.1
Vanillic acid	−6.4	−5.4	−6.1
Salicylic acid	−6.2	−6.1	**−8.0** (-7.7)[i]
Galangin	**−8.0**	−6.9	**−7.3**
S-eriodictyol	**−8.4**	−7.2	−6.7
Caffeic acid	−6.8	−5.7	−6.6
Fisetin	**−8.7**	−6.8	—
Oleanolic acid[b]	**−8.1**	−7.3	**−5.6** (-5.6)[d] (-5.8)[e]
Kojic acid[c]	—	—	(-5.5)[f]
Tropolone	—	—	**−5.8** (-3.2)[g] (-4.8)[h] (-4.9)[f]

Bold values are the most active compounds; [a] Binding energy indicate binding affinity for the active site into tyrosinase enzyme; [b]Oleanolic acid was used as a positive control for anti-collagenase and anti-elastase activity; [c]Kojic acid was used as a positive control for anti-tyrosinase activity; [d]Predicted binding score reported by (Azami et al., 2017); [e]Predicted binding score reported by (Liu et al., 2018); [f] Predicted binding score reported by (Karakaya et al., 2019); [g]Predicted binding score reported by (Asadzadeh et al., 2015); [h]Predicted binding score reported by (Nokinsee et al., 2015); [i]Predicted binding score reported by (Chung et al., 2018).

HIS218 residues and numerous hydrophobic interactions between *S*-eriodictyol and ALA182, LEU235, PHE242, LEU181, GLY179, LEU235 were also observed. Fisetin was found to best bind with human collagenase (binding energy −8.7 kcal/mol) exhibiting the highest collagenase affinity than inhibitor oleanolic acid (-8.1 kcal/mol). Their high affinity is a consequence of fisetin displayed one hydrogen bonding interaction with key aminoacid GLU219 into the catalytic domain of collagenase, one strong π − anion contact between aryl moiety with anionic amino acid GLU219 and several hydrophobic interactions formed with ALA182, LEU181, SER239, LEU235, ALA216, GLY178, ALA184. Here, anti-collagenase docking results revealed some bioactive compounds from ethanol extract of *P. edulis* seeds, which might have synergistic effect against collagenase as a possible molecular mechanism correlating reasonably well the collagenase assay with docking studies.

3.4.2. Tyrosinase docking profile

A second analysis consisted in the simulation of the active compound galangin in comparison with Kojic acid and Tropolone as current inhibitors into the cleavage site of Tyrosinase. To compare the best binding pose of galangin with the well-known inhibitors of tyrosinase (Kojic acid and Tropolone), Fig. 4 illustrates the most stable binding poses based on AutoDock scoring listed in Table 1 into the catalytic domain of tyrosinase (binuclear copper-containing domain). The superposition of the inhibitor Kojic acid (*in violet*) and Tropolone (*in hotpink*) and the best conformation obtained theoretically for galangin, showed that the flexible ligand (obtained by docking simulation) can accommodate themselves into stable conformations occupying this cleavage binding site during docking process.

The results of molecular docking studies reveal that galangin has great potential to inhibit tyrosinase, indicated by the high binding affinity (docking score −8.0 kcal/mol). The results showed that the interaction energy of galangin was better than the positive control Kojic acid (-5.6 kcal/mol) and inhibitor tropolone (-5.68 kcal/mol). Our docking data obtained for kojic acid demonstrated once again that affinity on tyrosinase for kojic acid is conditioned by its capacity to bind different histidine residues of the catalytic triad into bi-nuclear copper center, as shown in the Fig. 5B. On the other side, when explored the predicted best conformation for galangin in the mushroom tyrosinase binding site (Fig. 5B), we observed several interactions especially the interaction with at least one of the key catalytic residues, which stabilizes the catalytic site and may contribute to inhibitory activity. Thus, galangin showed key π-π contact between aryl group and HIS263 residue which is part of catalytic triad and support the stability of ligand–protein complex into mushroom tyrosinase catalytic domain. Despite most of the compounds (including galangine) does not interact with the bi-nuclear copper ions, the greatest score (more than current inhibitors) and non-covalent contact with HIS263 suggest that the majoritarian compounds from ethanol extract of *P. edulis*, specially galangin can both block the Cu^{2+}/Cu^{+} redox cycle that is essential for the catalytic activity of tyrosinase by their effectiveness intercalation into the cleavage pocket and disrupting the noncovalent interactions between the coppers atoms and the histidine-based catalytic triad, but not the bi-nuclear copper center directly. We founded that is a major contributor to the binding of these phytochemical compounds, particularly galangin to this metalloproteinase active site.

To support this observation, further analysis into the catalytic pocket was carried out. First, we founded that galangin fit close to binuclear copper-containing domain displayed distances between the 5-hydroxyl group (flavone ring) and both Cu^{2+} ions < 3.3 Å (Fig. 5C), which might hinder the access of their substrates to the active site copper ions. Second, several strong non-covalent interactions were found for all investigated compounds. We focused special attention on those of galangine (has the highest binding energy), which form two strong hydrogen bond interactions between the hydroxyl groups in a flavone ring with ASN260 and MET280 residues, respectively. What is more, four π-stacking contacts were formed between molecules and the PHE264, SER282, VAL283, ALA286 residues, respectively, which stabilizes its orientation in the catalytic cavity. In addition, galangin formed multiple hydrophobic interactions with crucial residues, among those ALA287, PHE264, GLY281, GLY267, PHE90, GLY86, that confer stability to complex during the binding event. Finally, these docking findings revealed all investigated compounds, specially galangin could act as competitive inhibitors of mushroom tyrosinase into the cleavage pocket and could support the effectiveness of ethanol extract of *P. edulis* during *in vitro* tyrosinase assay (IC_{50} = 141.3 μg/mL).

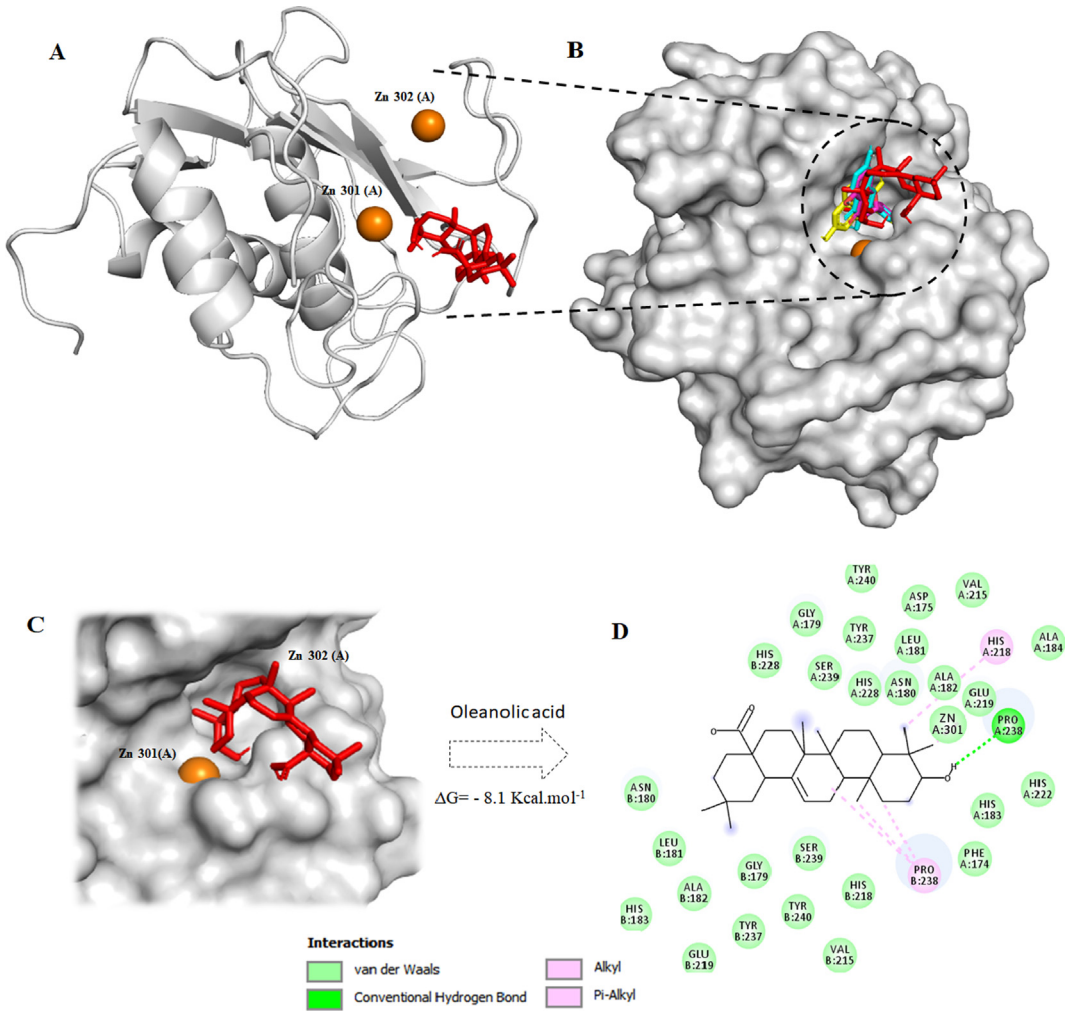

Fig. 2 **(A)** Oleanolic acid into collagenase cleavage pocket **(B)** Superposition of the best conformation of the most docking-active components **galangin** (*in yellow*), ***S*-eriodictyol** (*in magenta*), **fisetin** (*in cyan*) as well as **oleanolic acid** (*in red*) as potent collagenase inhibitor. **(C)** The best conformation of the potent collagenase inhibitor oleanolic acid into collagenase cleavage active site **(D)** 2D ligand-protease interaction plot between the inhibitor oleanolic acid with collagenase. Dashed lines indicate interactions of oleanolic acid with collagenase enzyme.

3.5. Molecular dynamics (MD) simulations and calculations of the free energy of binding

In order to demonstrated the stability of the most docking active compounds (fisetin and galangine) into the catalytic domain of collagenase and tyrosinase, respectively, the docked structures served as starting structures for MD simulations by using the Gromacs program (Abraham et al. 2015). Then, MD simulations were performed to check changes in conformation and permanency of the fisetin in complex with collagenase and galangin into tyrosinase domain cleft, respectively. To this aim, the root means square deviation (RMSD) was calculated for fisetin and galangin after 40 ns of MD simulation at real natural conditions (aqueous solution at T = 25 °C, p = 1 atm) inside catalytic binding pocket of collagenase and tyrosinase on an individual basis. Overall, in contrast with the initial docking pose, RMSD numbers (Fig. 6A and 6C) for carbon-alpha and backbone atoms in the collagenase and tyrosinase, metal ions, as well as ligands (fisetin and galangin) atoms, showed small fluctuations demonstrating the stability of these complexes during 40 ns simulation.

As illustrated in Fig. 6, calculated RMSD values for fisetin and galagine into enzymes active site fall within the ideal range around 2 Å (smaller RMSD values indicate higher stability of the simulation) (Gohlke et al., 2000; Kramer et al., 1999). Thus, the RMSD of the backbone of fisetin into the binding pocket on collagenase was 2.63 ± 0.82 Å, whereas galangine displayed a lowest RMSD value of 0.47 ± 0.14 Å inside tyrosinase catalytic domain. On the other side, the position of zinc and copper ions was very stable during the MD simulations as the average maximum RMSDs of these atoms is about 0.505 Å ± 0.125. The comparative analyses showed that fisetin exhibited higher fluctuated peaks into collagenase catalytic cleft when compared to galangine, meaning galangine is more stable throughout the simulation time period into tyrosinase binding pocket. Additionally, the fisetin RMSD indicated that the compound gradually stabilized after 5 ns, which is an indication of its higher flexibility within the catalytic binding site

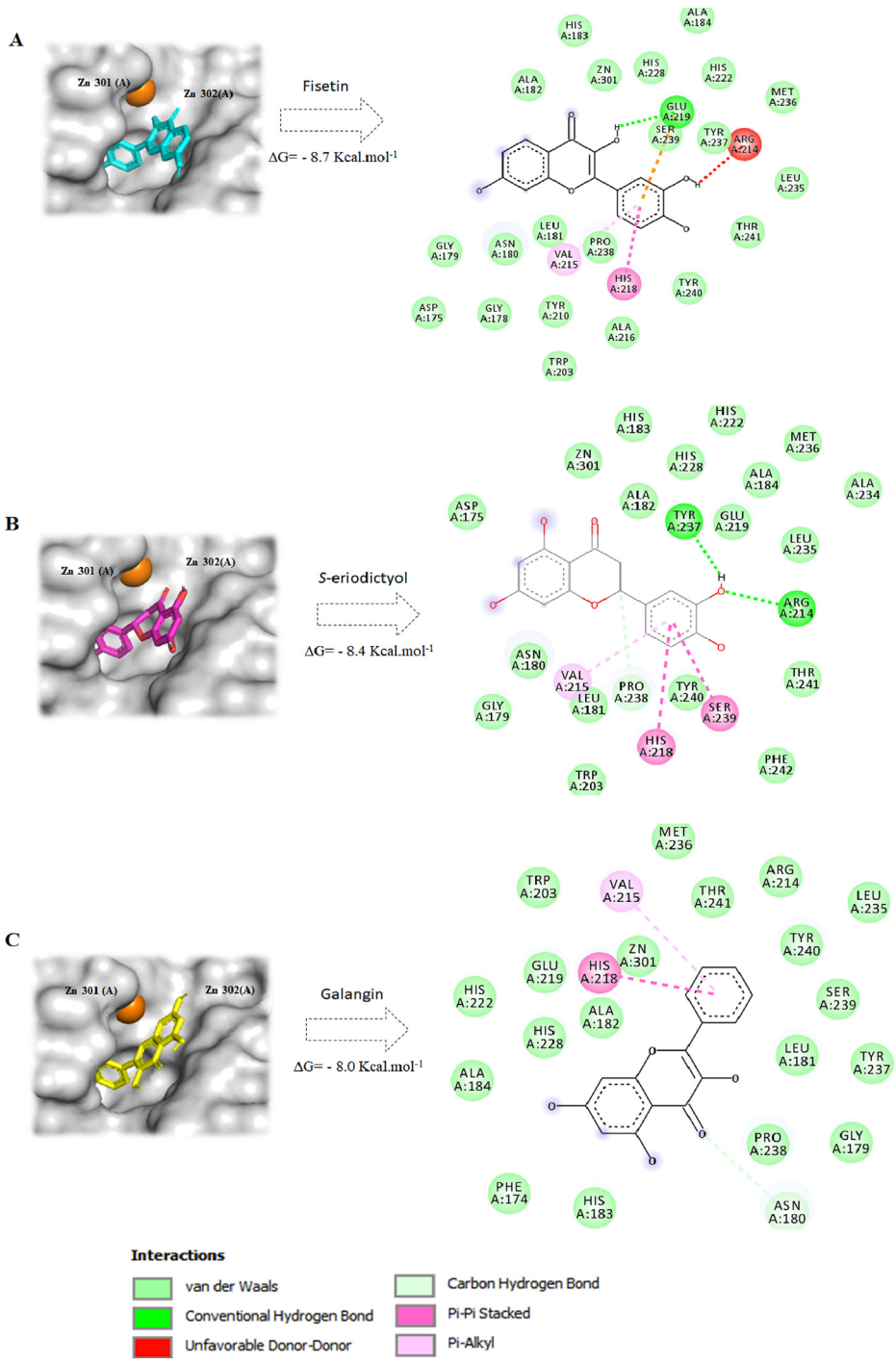

Fig. 3 **(A-C)** The best conformation of the three active components within catalytic pocket of collagenase (PDB: 1CGL). 2D interaction modes plots between the selected compounds with collagenase. Interactions between each component and amino acids residues into collagenase binding domain are indicated by the dashed lines.

on collagenase compared to galangin which to acquire the stability beyond 2 ns into the tyrosinase catalytic site. Furthermore, a rigorous analysis of the 2D-interactions plots after MD run, showed that fisetin conserved two key interactions with histidine residues of the catalytic triad (HIS228 and HIS218), which contributes to the stability of ligand–protein complex. Galangine display the same behavior, which retains contacts very close to HIS263, HIS259 and HIS85 in comparison to the initial docking pose. In this scenario, despite slight conformational changes that were observed during simulation, the computational MD studies further revealed that fisetin and galangine still maintain several important protein–ligand contacts into the metal binding sites in comparison to the initial docking conformations (see supporting information in figures S1 and S2). Thus, 2D-interactions plot determined by MD simulations for collagenase-fisetin showed five

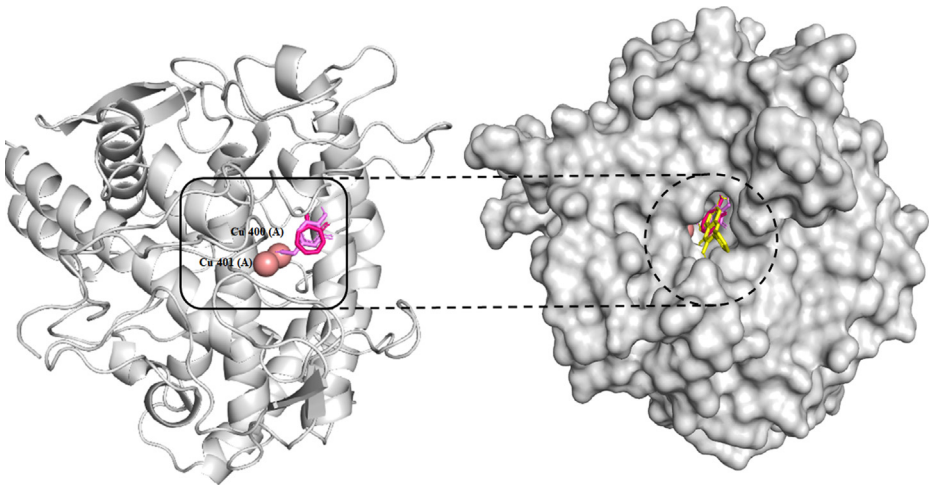

Fig. 4 Superposition of the best conformation of galangin (*in yellow*) as well as two well-known inhibitors: kojic acid (*in violet*) and tropolone (*in hotpink*) alongside the tyrosinase catalytic pocket (PDB: 2Y9X).

conserved residues as follow: LEU181, GLU219, PRO238, TYR237 and SER239. Meanwhile, tyrosinase-galangin interaction map predicted during 40 ns of MD simulation showed interactions with VAL283, MET280, ALA286, GLY281, PHE264, SER282, GLU256 residues through hydrogen bonds and hydrophobic interactions; Interestingly, after MD simulation it was founded that galangine also displayed a key contact very close to Cu (201), which the copper ion is bi-coordinated with hydroxyl and cetonic groups (flavone ring) within 2.70 Å of distance, that interaction could play a crucial role in the inhibitory effect of extract against tyrosinase. The radius of gyration (Rg) represents the compactness of the protein structure and conformational stability of the whole systems (i.e., protein–ligand complexes). Apart from RMSD, Rg we also plotted to observe the conformational alterations and dynamic stability of the fisetin and galangin into the catalytic sites. The predicted values of Rg for fisetin (3.64 ± 0.02 Å) and galangin (3.34 ± 0.02 Å) is showed in Fig. 6B and 6D, respectively. Rg values confirm the stabilization and suggest there was no significant change in the residual backbone and folding of the collagenase and tyrosinase after the ligands binding process.

According to the aforementioned, after MD simulations the binding interactions initially shown by the docking results were maintained and the ligands remained stable in the catalytic site compared to the initial docking conformation. In this scenario, in order to compare the best conformation poses from MD simulation and docking, we plotted the superposition of the docked complex 3D-structures before and after the MD simulation into the catalytic cavity (see supporting information in figures S3 and S4). In general, minor differences between the structure extracted after 50-ns MD simulation and the docking pose of both ligands were observed. In comparison to initial dock conformation, fisetin only manifested a slight rotational motion of the flavone ring during MD simulation, whereas for galangin a small horizontal displacement of 1.16 Å for flavone ring was evidenced. MD results suggest the conformation of the binding pocket and both ligands were stable during 40 ns of MD simulations, suggesting the rationality and validity of our docking studies.

Findings from MD simulations above-mentioned were further quantified using the semi-macroscopic method, namely Molecular Mechanics Poisson–Boltzmann/Surface Area (MM/PBSA). This current computational approach should provide a guide for rational drug design estimating the free energy of the binding of small ligands to biological macromolecules. MM/PBSA method allows a molecular understanding of the binding interaction between ligand to the potential target by estimating different components of interaction energy that contributes to this binding (Genheden and Ryde, 2015; Singh and Warshel, 2010). Therefore, MM/PBSA calculations were performed in order to obtain free energies of the complex fisetin-collagenase and galangin-tyrosinase, which are shown in Table 4.

From MM-PBSA results, fisetin possesses optimal nonbonded interaction energy with collagenase indicating its strong binding affinity, revealing a value of −13.42 ± 0.04 kc al.mol^{-1}. Further, the obtained values indicated that the contribution of nonbonded interactions energies such as van der Waals was more significant than that of the electrostatic energy, playing a significant role in the inhibition into the cleavage site collagenase.

This demonstrated once again, the importance of hydrophobic contacts found when fisetin was docked to the collagenase and provide strong evidence for both their specific heavy binding and how collagenase-fisetin complex stabilized inside the catalytic domain. Poor contribution of polar solvation energy for fisetin binding is observed by the positive value obtained after MM-PBSA runs (24.40 ± 0.03 kcal.mol^{-1}). Additionally, MM-PBSA approach showed that six residues ASN180, LEU181, VAL215, PRO238, SER239 and TYR240 contributed positively to the binding free energy of fisetin, resulting to be consistent with those findings founded in docking and MD simulations. Interestingly, no significant contribution in the complex stability was found for GLU219, HIS218, HIS222 and ARG214 which display positive energy suggesting nonfavorable interactions of Fisetin with these collagenase residues. The contribution of every residue in fisetin binding was explored and reported in Figure S5 of the Supporting Information.

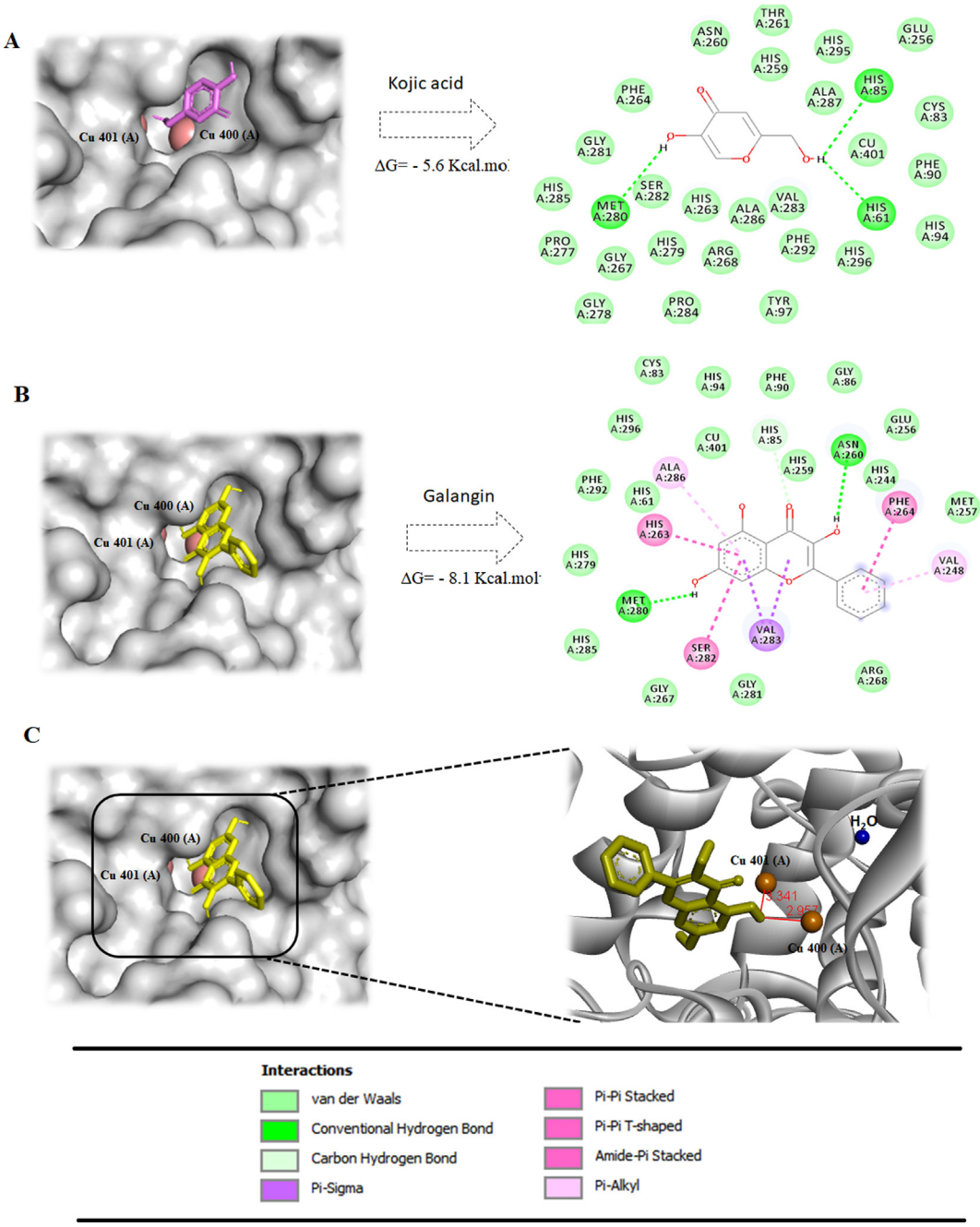

Fig. 5 **(A-B)** The best conformation of galangin and the inhibitor kojic acid within catalytic pocket of mushroom tyrosinase (PDB: 2Y9X) and 2D interaction modes plots between the selected ligands with tyrosinase. Interactions between each component and amino acids residues into tyrosinase cleavage domain are indicated by the dashed lines. **(C)** Distances in ångströms between the galangin and Cu environment into tyrosinase catalytic domain.

On other hand, MM-PBSA score for galangin exhibited a binding energy value of -17.23 ± 0.03 kcal.mol^{-1} signifying its strong binding affinity on tyrosinase (Table 2). The obtained value indicated that the contribution of van der Waals interaction was much larger than the electrostatic energy. After MM-GBSA runs, a little contribution of polar solvation energy to the galangin binding with tyrosinase was observed by the positive value obtained (14.10 ± 0.01 kcal. mol-1). We also explored the hotspot residues of tyrosine which had more influence on the predicted binding affinity with galangin. Interestingly, MM/PBSA predicts great contribution to the interaction of galangin with the key residues HIS85, HIS259 and HIS263 which is part of binuclear copper-containing catalytic domain on tyrosinase enzyme and were also evident in the MD simulations, making them the major contributors to binding free energy. Further, PHE264, VAL283, VAL248, HIS279, ASP269, MET280, GLY281 and SER282 residues had a positive contribution to galangin affinity suggesting that they would play a key role in the binding event. But three residues had strong repulsive

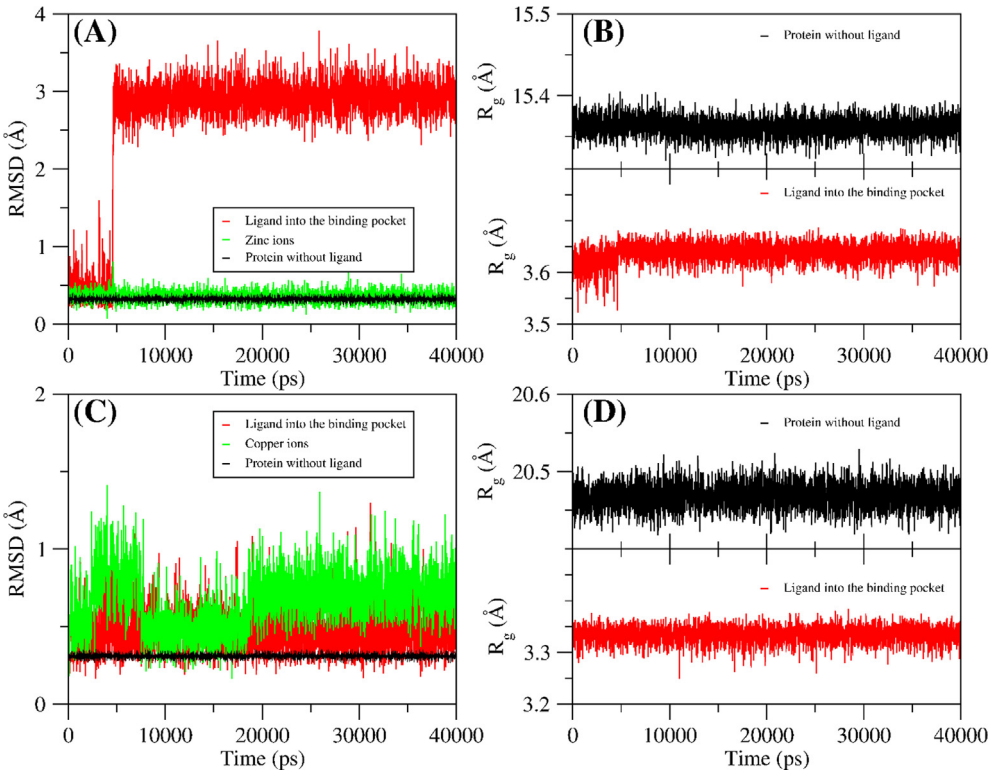

Fig. 6 **(A)** RMSD of the backbone of Fisetin into the collagenase active site (*red*), protein without ligand (*black*) and Zinc ions (*green*) **(B)** Radius of gyration (Rg) plot for Fisetin into the binding pocket (*red*) and protein without ligand (*black*) **(C)** RMSD of the backbone of galangin into the tyrosinase catalytic pocket (*red*), protein without ligand (*black*) and Copper ions (*green*) **(D)** Radius of gyration (Rg) plot for galangin into the binding pocket (*red*) and protein without ligand (*black*).

Table 4 Protein-ligand binding free energy, ΔG in kcal mol^{-1}. Average obtained from 3501 snapshots MD trajectory using the MM-PBSA method with the *g_mmpbsa* software.

Ligand	van der Waals energy	Electrostatic energy	Polar solvation energy	SASA energy	Binding energy
Fisetin	−34.27 ± 0.03	−0.69 ± 0.02	24.40 ± 0.03	−2.85 ± 0.00[a]	−13.42 ± 0.04
Galangin	−30.19 ± 0.03	1.80 ± 0.01	14.10 ± 0.01	−2.94 ± 0.00[a]	−17.23 ± 0.03

[a] A result of the order of 1×10^{-3} was obtained.

effects for the interaction of galangin with tyrosinase (namely, GLU256, ASN260 and ARG268), contributing unfavorably towards the total free energy. Each residue contribution in galangin binding is listed in Figure S5 of the Supporting Information.

Based on findings from molecular dynamics and the binding energy-MM-PBSA studies, we observed that some secondary metabolic compounds found in the ethanol extract of *P. edulis* present marked interaction to the age-related enzymes (specially, Collagenase and Tyrosinase), being itself strong evidence that key amino acids for activating of these enzymes well-recognizes these substrates, explaining its inhibitory effect. From our results, we believe that the ethanol extract of *P. edulis* should be taken into consideration as a future promise for further development of anti-aging cosmetics through strong inhibition of aging-associated enzymes.

3.6. Calculation of cosmeceutical drug-likeness indices and scoring

Calculated cosmeceutical drug-likeness profiles play a critical role in assessing the quality of novel anti-aging candidates. Early predictions of the pharmacokinetic behavior of the promising antiaging compounds based on its structure could help to find safer and effective leads for preclinical topical testing. Here, we calculated and analyzed various drug-likeness indices for the most qualified components on an ethanol extract of *P. edulis* (Table 5). So, nine pharmacokinetics parameters were calculated as cosmeceutical drug-likeness filter for genistein, protocatechuic acid, vanillic acid, salicylic acid, galangin, *S*-eriodictyol, caffeic acid, fisetin and compared to those inhibitors oleanolic acid and kojic acid, respectively. Results would demonstrate the feasibility of the selected

Table 5 *In silico* cosmeceutical pharmacokinetic indices and reported acute toxicity for the main constituents in ethanol extract of *P. edulis*.

Compound	M.W [a]	n-OHNH [b]	n-ON [c]	Log $P_{o/w}$ [d]	Log S_w [e]	Predicted dermatopharmacokinetic (DPK) *indices*					Oral Toxicity (LD_{50} mg/kg mouse)[j]
						Log K_p (cm/h)[f]	D_{de} (cm^2/s) $\times 10^{-7}$ g	Log J_{max} [h] mole·cm^{-2}·h^{-1}	Log $K_{sc/w}$ [i]	Transdermal Rule of five	
Genistein	270.241	2.0	3.75	1.679	−3.024	−3.196	1.074	−9.034579	1.04	0	> 500
Protocatec A.	154.122	3.0	3.50	0.014	−0.788	−3.680	1.883	−6.828318	−0.14	1	> 800
Vanillic acid	168.149	2.0	3.50	1.020	−1.302	−3.042	1.726	−7.094831	0.48	1	> 2691
Salicylic acid	138.123	1.0	1.75	2.251	−1.595	−1.984	2.101	−6.524337	1.12	1	> 891
Galangin	270.241	2.0	3.75	1.765	−3.351	−3.135	1.074	−9.034579	1.09	0	> 1500
S-eriodictyol	288.256	3.0	4.75	0.921	−3.089	−4.498	1.007	−9.376864	0.10	0	—
Caffeic acid	180.160	3.0	3.50	0.519	−1.255	−3.839	1.611	−7.32304	−0.08	1	> 721
Fisetin	286.240	4.0	5.00	0.468	−2.856	−4.486	1.014	−9.33856	0.09	0	> 500
Oleanolic A.	456.707	2.0	3.70	5.914	−6.597	−1.327	0.635	−12.57743	3.68	2	> 800
Kojic acid	142.111	2.0	4.00	−0.630	−0.411	−4.054	5.955	−6.600109	−0.14	1	> 2691

a Molecular weight of the molecule ≤ 300; b n-OHNH number of hydrogen bonds donors ≤ 5; c n-ON number of hydrogen bond acceptors < 5; dPredicted octanol–water partition coefficient < 2.6; ePredicted of solute aqueous solubility > − 2.3; fSkin permeation coefficient of chemical in the stratum corneum; gEffective diffusion coefficient in dermis M.W-based; [h] Solute maximum percutaneous flux across human skin > -2.52. [i] Stratum corneum/water partition coefficient. [j]Experimental value from PubChem Data Base. Extremely toxic (< 5); Highly toxic (5–50); Moderately toxic (50–500); Slightly toxic (500–5000); Practically non-toxic (5000–15000); Relatively harmless (> 15000).

components from the ethanol extract of *P. edulis* seeds as suitable cosmetic drugs.

Our findings showed that all selected phenolic compounds had drug-like characteristics and within the range in comparison to FDA-approved transdermal drugs. Compounds display at least one violation of Transdermal Rule of five compared to oleanolic acid (which presented two violations) and kojic acid (presented one violation) making ethanol extract of *P. edulis a newer* potential therapeutic option for anti-aging formulations development. In this scenario, studied compounds displayed optimal values for $LogS_w$ (ranging from −3.351 to −2.856), MW (< 288 Da), H-bond donors (< 4), H-bond acceptors (< 5) and $LogP_{o/w}$ (ranging from 0.014 to 2.251) in comparison with those FDA-approved transdermal drugs (for more details readers can refer to Table 2). These results, demonstrating ethanol extract of *P. edulis* can penetrate through the skin easily, one of the most important determinants after topical applications.

Finally, to demonstrate the potential of ethanol extract of *P. edulis* seeds as promissory cosmeceutical, skin permeation indices of the main phenolic compounds present were studied. So, four essential physicochemical transdermal properties involved in the development of cosmetic anti-aging formulations were calculated (namely, Log K_p, D_{de}, Log J_{max} and Log $K_{sc/w}$). Calculated $LogJ_{max}$, which explains delivery or flux of solutes into or through the skin after topical applications, revealed ideal values for selected phenols in comparison to those FDA-approved transdermal drugs (> −2.52 mol·cm^{-2}·h^{-1}). The logarithmic values of skin permeation coefficient (LogKp) were comparable to some conventional topical drugs (ranging from −1.262 to −3.931) ranging between −1.984 and −4.498. Suitable values for percutaneous absorption (Log P_{ab}) and effective diffusion coefficient in dermis (D_{de}) were determined. Notably, fisetin and galangin above-mentioned by its promissory docking numbers showed good cosmeceutical pharmacokinetic indices, due to Transdermal Rule of five was not violated and both displayed optimum partition and diffusion values into skin within the ideal ranged of the known typical drugs FDA-approved for transdermal administration. On the other hand, the oral toxicity (LD_{50} mg/kg mouse) reported to the most phenolic compounds identified in the extract, showed LD_{50} toxicity values > 500 mg/kg. This could presumably explain why ethanol extract of *P. edulis* did not exhibit cytotoxicity when it was evaluated on blood cells between 1000 y 4000 μg/mL, where cellular viability was similar to the control (100% viability). Furthermore, it is important to highlight that concentrations evaluated in the cytotoxicity test were higher than those concentrations where the extract has a bioactive effect of interest at the antioxidant level and on the inhibition of the enzymes related to skin aging processes evaluated in this study, which could guarantee the safe use of the extract in cosmetic applications for the skin. Finally, integrating enzymatic studies with multi-level modeling approaches we demonstrated that the ethanol extract of *P. edulis* by itself and some of its components could be considered as an attractive safe option for antiaging topical preparations.

4. Conclusions

Here, we used integration of *in vitro* and *in silico* perspectives to explain potential anti-aging effects of *P. edulis* and propose

its ethanol extract as a pharmacologically active source useful in functional cosmeceutical formulations. The ethanol extract from the seeds of *P. edulis* proved may to be a safe valuable resource for skin aging therapy, containing a considerable concentration of simple phenols and mainly flavonoid aglycone, which is associated with its antioxidant activity and with the *in vitro* inhibition of the enzymes collagenase, elastase, and tyrosinase observed in this work. Furthermore, multi-level computational approaches demonstrated that various constituents of *P. edulis* displayed docked conformations into the cleavage site for these enzymes compared to structure orientation of current inhibitor oleanolic acid, kojic acid and tropolone, respectively. Among them, fisetin, *S*-eriodictyol and galangin fitted well in the catalytic pocket and showed the lowest binding score than approved inhibitors. Therefore, these compounds are probably bound to age-related enzymes with the same binding mode as the current inhibitors in the crystal complexes. Under the above-mentioned, we encourage strong use of ethanol extract from *P. edulis* as a new safe alternative for anti-aging therapy because both several of its components showed good inhibitory potency and marked binding affinity to the age-related enzymes, and had good antioxidant properties. On the other hand, we expect that our findings obtained in this study will facilitate future developments of new antiaging cosmeceuticals based on age-related enzymes inhibition. However, experimental validation of *in silico* predictions and some clinical testing are needed before it comes to be used in future clinical applications.

Acknowledgements

This study was supported by the Universidad de Antioquia, Universidad del Tolima and Universidad de Pamplona-Colombia.

References

Abraham, G., 2014. Unpredictable Systemic Risks to Topical Drugs. J. Drug Metab. Toxicol. 05, 7609. https://doi.org/10.4172/2157-7609.1000e122.

Abraham, M.J., Murtola, T., Schulz, R., Páll, S., Smith, J.C., Hess, B., Lindah, E., 2015. Gromacs: High performance molecular simulations through multi-level parallelism from laptops to supercomputers. SoftwareX 1–2, 19–25. https://doi.org/10.1016/j.softx.2015.06.001.

Alberto Checa Rojas, 2018. Método: aislamiento de células sanguíneas por gradiente de Ficoll-Paque [WWW Document]. Conogasi, Conoc. para la vida. URL http://conogasi.org/articulos/metodo-aislamiento-de-celulas-sanguineas-por-gradiente-de-ficoll-paque/ (accessed 6.11.20).

Alikhan, F.S., Maibach, H., 2011. Topical absorption and systemic toxicity. Cutan. Ocul. Toxicol. https://doi.org/10.3109/15569527.2011.560914.

Arda, O., Göksügür, N., Tüzün, Y., 2014. Basic histological structure and functions of facial skin. Clin. Dermatol. https://doi.org/10.1016/j.clindermatol.2013.05.021.

Asadzadeh, A., Fassihi, A., Yaghmaei, P., Pourfarzam, M., 2015. Docking studies of some novel Kojic acid Derivatives as possible tyrosinase inhibitors. Biomed. Pharmacol. J. 8, 535–545. https://doi.org/10.13005/bpj/796.

Azami, F., Tazikeh-Lemeski, E., Mahmood-Janlou, M.-A., 2017. Kojic Acid Effect on the Inhibitory Potency of Tyrosinase. J. Chem. Heal. Risks 7, 147–155. https://doi.org/10.22034/JCHR.2017.544176.

Baumann, L., 2007. Skin ageing and its treatment. J. Pathol. https://doi.org/10.1002/path.2098.

Bayly, C.I., Cieplak, P., Cornell, W.D., Kollman, P.A., 1993. A well-behaved electrostatic potential based method using charge restraints for deriving atomic charges: The RESP model. J. Phys. Chem. 97, 10269–10280. https://doi.org/10.1021/j100142a004.

Blume-Peytavi, U., Kottner, J., Sterry, W., Hodin, M.W., Griffiths, T. W., Watson, R.E.B., Hay, R.J., Griffiths, C.E.M., 2016. Age-associated skin conditions and diseases: Current perspectives and future options. Gerontologist. https://doi.org/10.1093/geront/gnw003.

Brand-Williams, W., Cuvelier, M.E., Berset, C., 1995. Use of a free radical method to evaluate antioxidant activity. LWT - Food Science and Technology 28, 25–30. https://doi.org/10.1016/S0023-6438(95)80008-5.

Bravo, K., Alzate, F., Osorio, E., 2016. Fruits of selected wild and cultivated Andean plants as sources of potential compounds with antioxidant and anti-aging activity. Ind. Crops Prod. 85, 341–352. https://doi.org/10.1016/j.indcrop.2015.12.074.

Bravo, K., Duque, L., Ferreres, F., Moreno, D.A., Osorio, E., 2017. Passiflora tarminiana fruits reduce UVB-induced photoaging in human skin fibroblasts. J. Photochem. Photobiol. B Biol. 168, 78–88. https://doi.org/10.1016/j.jphotobiol.2017.01.023.

Bravo, K., Sepulveda-Ortega, S., Lara-Guzman, O., Navas-Arboleda, A.A., Osorio, E., 2015. Influence of cultivar and ripening time on bioactive compounds and antioxidant properties in Cape gooseberry (Physalis peruviana L.). J. Sci. Food Agric. 95, 1562–1569. https://doi.org/10.1002/jsfa.6866.

Bunge, A.L., Cleek, R.L., 1995. A New Method for Estimating Dermal Absorption from Chemical Exposure: 2. Effect of Molecular Weight and Octanol-Water Partitioning. Pharm. Res. An Off. J. Am. Assoc. Pharm. Sci. 12, 88–95. https://doi.org/10.1023/A:1016242821610.

Carciochi, R.A., D'Alessandro, L.G., Vauchel, P., Rodriguez, M.M., Nolasco, S.M., Dimitrov, K., 2017. Valorization of Agrifood By-Products by Extracting Valuable Bioactive Compounds Using Green Processes, in: Grumezescu, A.M., Holban, A.M.B.T.-I.E. by P.M. in F. (Eds.), Ingredients Extraction by Physicochemical Methods in Food. Elsevier, pp. 191–228. https://doi.org/10.1016/B978-0-12-811521-3.00004-1.

Chen, L., Han, L., Saib, O., Lian, G., 2015. In Silico Prediction of Percutaneous Absorption and Disposition Kinetics of Chemicals. Pharm. Res. 32, 1779–1793. https://doi.org/10.1007/s11095-014-1575-0.

Choy, Y. Bin, Prausnitz, M.R., 2011. The rule of five for non-oral routes of drug delivery: Ophthalmic, inhalation and transdermal. Pharm. Res. https://doi.org/10.1007/s11095-010-0292-6.

Chung, K.W., Jeong, H.O., Lee, E.K., Kim, S.J., Chun, P., Chung, H. Y., Moon, H.R., 2018. Evaluation of antimelanogenic activity and mechanism of galangin in silico and in vivo. Biol. Pharm. Bull. 41, 73–79. https://doi.org/10.1248/bpb.b17-00597.

Cornell, W.D., Cieplak, P., Bayly, C.I., Gould, I.R., Merz, K.M., Ferguson, D.M., Spellmeyer, D.C., Fox, T., Caldwell, J.W., Kollman, P.A., 1995. A Second Generation Force Field for the Simulation of Proteins, Nucleic Acids, and Organic Molecules. J. Am. Chem. Soc. 117, 5179–5197. https://doi.org/10.1021/ja00124a002.

Corrêa, R.C.G., Peralta, R.M., Haminiuk, C.W.I., Maciel, G.M., Bracht, A., Ferreira, I.C.F.R., 2016. The past decade findings related with nutritional composition, bioactive molecules and biotechnological applications of Passiflora spp. (passion fruit). Trends Food Sci. Technol. 58, 79–95. https://doi.org/10.1016/j.tifs.2016.10.006.

Corrêa, R.C.G., Peralta, R.M., Haminiuk, C.W.I., Maciel, G.M., Bracht, A., Ferreira, I.C.F.R., 2018. New phytochemicals as potential human anti-aging compounds: Reality, promise, and challenges. Crit. Rev. Food Sci. Nutr. https://doi.org/10.1080/10408398.2016.1233860.

Czekanska, E.M., 2011. Assessment of cell proliferation with resazurin-based fluorescent dye. Methods Mol. Biol. 740, 27–32. https://doi.org/10.1007/978-1-61779-108-6_5.

Darden, T., York, D., Pedersen, L., 1993. Particle mesh Ewald: An N·log(N) method for Ewald sums in large systems. J. Chem. Phys. 98, 10089–10092. https://doi.org/10.1063/1.464397.

de Santana, F.C., de Oliveira Torres, L.R., Shinagawa, F.B., de Oliveira e Silva, A.M., Yoshime, L.T., de Melo, I.L.P., Marcellini, P.S., Mancini-Filho, J., 2017. Optimization of the antioxidant polyphenolic compounds extraction of yellow passion fruit seeds (Passiflora edulis Sims) by response surface methodology. J. Food Sci. Technol. 54, 3552–3561. https://doi.org/10.1007/s13197-017-2813-3.

Delpino-Rius, A., Eras, J., Vilaró, F., Cubero, M.Á., Balcells, M., Canela-Garayoa, R., 2015. Characterisation of phenolic compounds in processed fibres from the juice industry. Food Chem. 172, 575–584. https://doi.org/10.1016/j.foodchem.2014.09.071.

Ditchfield, R., Hehre, W.J., Pople, J.A., 1971. Self-consistent molecular-orbital methods. IX. An extended gaussian-type basis for molecular-orbital studies of organic molecules. J. Chem. Phys. 54, 720–723. https://doi.org/10.1063/1.1674902.

Duque, L., Bravo, K., Osorio, E., 2017. A holistic anti-aging approach applied in selected cultivated medicinal plants: A view of photoprotection of the skin by different mechanisms. Ind. Crops Prod. 97, 431–439. https://doi.org/10.1016/j.indcrop.2016.12.059.

Essmann, U., Perera, L., Berkowitz, M.L., Darden, T., Lee, H., Pedersen, L.G., 1995. A smooth particle mesh Ewald method. J. Chem. Phys. 103, 8577–8593. https://doi.org/10.1063/1.470117.

Farrokhnia, M., Mahnam, K., 2017. Molecular dynamics and docking investigations of several zoanthamine-type marine alkaloids as matrix metaloproteinase-1 inhibitors. Iran. J. Pharm. Res. 16, 173–186. https://doi.org/10.22037/ijpr.2017.1969.

Frisch, M.J., Pople, J.A., Binkley, J.S., 1984. Self-consistent molecular orbital methods 25. Supplementary functions for Gaussian basis sets. J. Chem. Phys. 80, 3265–3269. https://doi.org/10.1063/1.447079.

Gadioli, I.L., da Cunha, M. de S.B., de Carvalho, M.V.O., Costa, A. M., Pineli, L. de L. de O., 2018. A systematic review on phenolic compounds in Passiflora plants: Exploring biodiversity for food, nutrition, and popular medicine. Crit. Rev. Food Sci. Nutr. 58, 785–807. https://doi.org/10.1080/10408398.2016.1224805.

Genheden, S., Ryde, U., 2015. The MM/PBSA and MM/GBSA methods to estimate ligand-binding affinities. Expert Opin. Drug Discov. https://doi.org/10.1517/17460441.2015.1032936.

Gohlke, H., Hendlich, M., Klebe, G., 2000. Knowledge-based scoring function to predict protein-ligand interactions. Journal of Molecular Biology 295 (2), 337–356. https://doi.org/10.1006/jmbi.1999.3371.

González, L., Álvarez, A., Murillo, E., Guerra, C., Méndez, J., 2019. Potential uses of the peel and seed of passiflora edulis f. Edulis sims (Gulupa) from its chemical characterization, antioxidant and antihypertensive functionalities. Asian J. Pharm. Clin. Res. 12.

Greenwald, M.B.Y., Ben-Sasson, S., Bianco-Peled, H., Kohen, R., 2016. Skin redox balance maintenance: The need for an Nrf2-activator delivery system. Cosmetics. https://doi.org/10.3390/cosmetics3010001.

Grynkiewicz, G., Demchuk, O.M., 2019. New Perspectives for Fisetin. Front. Chem. https://doi.org/10.3389/fchem.2019.00697.

Guy, R.H., Potts, R.O., 1993. Penetration of industrial chemicals across the skin: A predictive model. Am. J. Ind. Med. 23, 711–719. https://doi.org/10.1002/ajim.4700230505.

Halper, J., Kjaer, M., 2014. Basic Components of Connective Tissues and Extracellular Matrix: Elastin, Fibrillin, Fibulins, Fibrinogen, Fibronectin, Laminin, Tenascins and Thrombospondins, in: Advances in Experimental Medicine and Biology. Springer, Dordrecht, pp. 31–47. https://doi.org/10.1007/978-94-007-7893-1_3.

Hariharan, P.C., Pople, J.A., 1973. The influence of polarization functions on molecular orbital hydrogenation energies. Theor. Chim. Acta 28, 213–222. https://doi.org/10.1007/BF00533485.

Hartanto, S., Lister, I.N.E., Fachrial, E., et al, 2019. A Comparative Study of Peel and Seed Extract of Passion Fruit (Passiflora edulis) as Anti Collagenase. Am. Sci. Res. J. Eng. Technol. Sci. 54, 42–48.

Hehre, W.J., Ditchfield, K., Pople, J.A., 1972. Self-consistent molecular orbital methods. XII. Further extensions of gaussian-type basis sets for use in molecular orbital studies of organic molecules. J. Chem. Phys. 56, 2257–2261. https://doi.org/10.1063/1.1677527.

Horst, J.A., Laurenzi, A., Bernard, B., Samudrala, R., 2012. Computational Multitarget Drug Discovery. Polypharmacology in Drug Discovery., 263–301 https://doi.org/10.1002/9781118098141.ch13.

Hui, X., Wester, R.C., Magee, P.S., Maibach, H.I., 1995. Partitioning of chemicals from water into powdered human stratum corneum (Callus): A model study. Vitr. Toxicol. J. Mol. Cell. Toxicol. 8, 159–167.

Irwin, J.J., Sterling, T., Mysinger, M.M., Bolstad, E.S., Coleman, R. G., 2012. ZINC: A free tool to discover chemistry for biology. J. Chem. Inf. Model. https://doi.org/10.1021/ci3001277.

Ismaya, W.T., Rozeboom, H.J., Weijn, A., Mes, J.J., Fusetti, F., Wichers, H.J., Dijkstra, B.W., 2011. Crystal structure of agaricus bisporus mushroom tyrosinase: Identity of the tetramer subunits and interaction with tropolone. Biochemistry 50, 5477–5486. https://doi.org/10.1021/bi200395t.

Jabłońska-Trypuć, A., Krętowski, R., Kalinowska, M., Świderski, G., Cechowska-Pasko, M., Lewandowski, W., 2018. Possible mechanisms of the prevention of doxorubicin toxicity by cichoric acid—antioxidant nutrient. Nutrients 10. https://doi.org/10.3390/nu10010044.

Jiménez-Atiénzar, M., Escribano, J., Cabanes, J., Gandía-Herrero, F., García-Carmona, F., 2005. Oxidation of the flavonoid eriodictyol by tyrosinase. Plant Physiol. Biochem. 43, 866–873. https://doi.org/10.1016/j.plaphy.2005.07.010.

Jiménez, N., Carrillo-Hormaza, L., Pujol, A., Álzate, F., Osorio, E., Lara-Guzman, O., 2015. Antioxidant capacity and phenolic content of commonly used anti-inflammatory medicinal plants in Colombia. Ind. Crops Prod. 70, 272–279. https://doi.org/10.1016/j.indcrop.2015.03.050.

Karakaya, G., Türe, A., Ercan, A., Öncül, S., Aytemir, M.D., 2019. Synthesis, computational molecular docking analysis and effectiveness on tyrosinase inhibition of kojic acid derivatives. Bioorg. Chem. 88,. https://doi.org/10.1016/j.bioorg.2019.102950 102950.

Kollman, P.A., Massova, I., Reyes, C., Kuhn, B., Huo, S., Chong, L., Lee, M., Lee, T., Duan, Y., Wang, W., Donini, O., Cieplak, P., Srinivasan, J., Case, D.A., Cheatham, T.E., 2000. Calculating structures and free energies of complex molecules: Combining molecular mechanics and continuum models. Acc. Chem. Res. 33, 889–897. https://doi.org/10.1021/ar000033j.

Koo, J.H., Hyoung, T.K., Yoon, H.Y., Kwon, K.B., Choi, I.W., Sung, H.J., Kim, H.U., Park, B.H., Park, J.W., 2008. Effect of xanthohumol on melanogenesis in B16 melanoma cells. Exp. Mol. Med. 40, 313–319. https://doi.org/10.3858/emm.2008.40.3.313.

Kramer, B., Rarey, M., & Lengauer, T. (1999). Evaluation of the FlexX incremental construction algorithm for protein- ligand docking. *Proteins: Structure, Function and Genetics*, *37*(2), 228–241. https://doi.org/10.1002/(SICI)1097-0134(19991101)37:2 < 228::AID-PROT8 > 3.0.CO;2-8

Kumari, R., Kumar, R., Lynn, A., 2014. G-mmpbsa -A GROMACS tool for high-throughput MM-PBSA calculations. J. Chem. Inf. Model. 54, 1951–1962. https://doi.org/10.1021/ci500020m.

Liu, H., Zhu, Y., Wang, T., Qi, J., Liu, X., 2018. Enzyme-Site Blocking Combined with Optimization of Molecular Docking for Efficient Discovery of Potential Tyrosinase Specific Inhibitors from Puerariae lobatae Radix. Molecules 23, 2612. https://doi.org/10.3390/molecules23102612.

Lourith, N., Kanlayavattanakul, M., 2013. Antioxidant activities and phenolics of Passiflora edulis seed recovered from juice production residue. J. Oleo Sci. 62, 235–240. https://doi.org/10.5650/jos.62.235.

Lourith, N., Kanlayavattanakul, M., Chingunpitak, J., 2017. Development of sunscreen products containing passion fruit seed extract.

Brazilian J. Pharm. Sci. 53. https://doi.org/10.1590/s2175-97902017000116116.

Lovejoy, B., Cleasby, A., Hassell, A.M., Longley, K., Luther, M.A., Weigl, D., McGeehan, G., McElroy, A.B., Drewry, D., Lambert, M.H., Jordan, S.R., 1994. Structure of the catalytic domain of fibroblast collagenase complexed with an inhibitor. Science 80-.). 263, 375–377. https://doi.org/10.1126/science.8278810.

Magnusson, B.M., Anissimov, Y.G., Cross, S.E., Roberts, M.S., 2004a. Molecular size as the main determinant of solute maximum flux across the skin. J, Invest. Dermatol. 122, 993–999. https://doi.org/10.1111/j.0022-202X.2004.22413.x.

Magnusson, B.M., Pugh, W.J., Roberts, M.S., 2004b. Simple rules defining the potential of compounds for transdermal delivery or toxicity. Pharm. Res. 21, 1047–1054. https://doi.org/10.1023/B:PHAM.0000029295.38564.e1.

Manzetti, S., McCulloch, D.R., Herington, A.C., van der Spoel, D., 2003. Modeling of enzyme-substrate complexes for the metalloproteases MMP-3, ADAM-9 and ADAM-10. J. Comput. Aided Mol. Des. 17, 551–565. https://doi.org/10.1023/B:JCAM.0000005765.13637.38.

Marvin - ChemAxon [WWW Document], 2007. URL https://chemaxon.com/products/marvin (accessed 6.11.20).

Matsui, Y., Sugiyama, K., Kamei, M., Takahashi, T., Suzuki, T., Katagata, Y., Ito, T., 2010. Extract of Passion Fruit (Passiflora edulis) Seed Containing High Amounts of Piceatannol Inhibits Melanogenesis and Promotes Collagen Synthesis. J. Agric. Food Chem. 58, 11112–11118. https://doi.org/10.1021/jf102650d.

Milewski, M., Stinchcomb, A.L., 2012. Estimation of maximum transdermal flux of nonionized xenobiotics from basic physicochemical determinants. Mol. Pharm. 9, 2111–2120. https://doi.org/10.1021/mp300146m.

Morris, G.M., Goodsell, D.S., Halliday, R.S., Huey, R., Hart, W.E., Belew, R.K., Olson, A.J., 1998. Automated docking using a Lamarckian genetic algorithm and an empirical binding free energy function. J. Comput. Chem. 19, 1639–1662. https://doi.org/10.1002/(SICI)1096-987X(19981115)19:14<1639::AID-JCC10>3.0.CO;2-B.

Morris, G.M., Ruth, H., Lindstrom, W., Sanner, M.F., Belew, R.K., Goodsell, D.S., Olson, A.J., 2009. AutoDock4 and AutoDockTools4: Automated docking with selective receptor flexibility. J. Comput. Chem. 30, 2785–2791. https://doi.org/10.1002/jcc.21256.

Mukherjee, P.K., Maity, N., Nema, N.K., Sarkar, B.K., 2011. Bioactive compounds from natural resources against skin aging. Phytomedicine 19, 64–73. https://doi.org/10.1016/j.phymed.2011.10.003.

Nokinsee, D., Shank, L., Lee, V.S., Nimmanpipug, P., 2015. Estimation of inhibitory effect against tyrosinase activity through homology modeling and molecular docking. Enzyme Res. 2015. https://doi.org/10.1155/2015/262364.

Oliveira, D.A., Angonese, M., Gomes, C., Ferreira, S.R.S., 2016. Valorization of passion fruit (Passiflora edulis sp.) by-products: Sustainable recovery and biological activities. J. Supercrit. Fluids 111, 55–62. https://doi.org/10.1016/j.supflu.2016.01.010.

Parrinello, M., Rahman, A., 1981. Polymorphic transitions in single crystals: A new molecular dynamics method. J. Appl. Phys. 52, 7182–7190. https://doi.org/10.1063/1.328693.

Pereira, M.G., Maciel, G.M., Haminiuk, C.W.I., Bach, F., Hamerski, F., de Paula Scheer, A., Corazza, M.L., 2019. Effect of Extraction Process on Composition, Antioxidant and Antibacterial Activity of Oil from Yellow Passion Fruit (Passiflora edulis Var. Flavicarpa) Seeds. Waste Biomass Valorization 10, 2611–2625. https://doi.org/10.1007/s12649-018-0269-y.

Polito, F., Marini, H., Bitto, A., Irrera, N., Vaccaro, M., Adamo, E.B., Micali, A., Squadrito, F., Minutoli, L., Altavilla, D., 2012. Genistein aglycone, a soy-derived isoflavone, improves skin changes induced by ovariectomy in rats. Br. J. Pharmacol. 165, 994–1005. https://doi.org/10.1111/j.1476-5381.2011.01619.x.

Ponec, M., Haverkort, M., Soei, Y.L., Kempenaar, J., Bodde, H., 1990. Use of Human Keratinocyte and Fibroblast Cultures for Toxicity Studies of Topically Applied Compounds. J. Pharm. Sci. 79, 312–316. https://doi.org/10.1002/jps.2600790408.

Potts, R.O., Guy, R.H., 1992. Predicting Skin Permeability. Pharm. Res. An Off. J. Am. Assoc. Pharm. Sci. 9, 663–669. https://doi.org/10.1023/A:1015810312465.

Rao, A.R., Sindhuja, H.N., Dharmesh, S.M., Sankar, K.U., Sarada, R., Ravishankar, G.A., 2013. Effective inhibition of skin cancer, tyrosinase, and antioxidative properties by astaxanthin and astaxanthin esters from the green alga haematococcus pluvialis. J. Agric. Food Chem. 61, 3842–3851. https://doi.org/10.1021/jf304609j.

Rittié, L., Fisher, G.J., 2002. UV-light-induced signal cascades and skin aging 1, 705–720.

Roothaan, C.C.J., 1951. New developments in molecular orbital theory. Rev. Mod. Phys. 23, 69–89. https://doi.org/10.1103/RevModPhys.23.69.

Sasaki, M., Horikoshi, T., Uchiwa, H., Miyachi, Y., 2000. Up-regulation of tyrosinase gene by nitric oxide human melanocytes. Pigment Cell Res. 13, 248–252. https://doi.org/10.1034/j.1600-0749.2000.130406.x.

Schmidt, M.W., Baldridge, K.K., Boatz, J.A., Elbert, S.T., Gordon, M.S., Jensen, J.H., Koseki, S., Matsunaga, N., Nguyen, K.A., Su, S., Windus, T.L., Dupuis, M., Montgomery, J.A., 1993. General atomic and molecular electronic structure system. J. Comput. Chem. 14, 1347–1363. https://doi.org/10.1002/jcc.540141112.

Schoellhammer, C.M., Blankschtein, D., Langer, R., 2014. Skin permeabilization for transdermal drug delivery: Recent advances and future prospects. Expert Opin. Drug Deliv. https://doi.org/10.1517/17425247.2014.875528.

Singh, N., Warshel, A., 2010. Absolute binding free energy calculations: On the accuracy of computational scoring of protein-ligand interactions. Proteins Struct. Funct. Bioinforma. 78, NA-NA. https://doi.org/10.1002/prot.22687.

Singh, U.C., Kollman, P.A., 1984. An approach to computing electrostatic charges for molecules. J. Comput. Chem. 5, 129–145. https://doi.org/10.1002/jcc.540050204.

Singleton, V.L., Orthofer, R., Lamuela-Raventós, R.M., 1999. Analysis of total phenols and other oxidation substrates and antioxidants by means of folin-ciocalteu reagent. Methods Enzymol. 299, 152–178. https://doi.org/10.1016/S0076-6879(99)99017-1.

Sivamani, P., Singaravelu, G., Thiagarajan, V., Jayalakshmi, T., Kumar, G.R., 2012. Comparative molecular docking analysis of essential oil constituents as elastase inhibitors. Bioinformation 8, 457–460. https://doi.org/10.6026/97320630008457.

Sousa Da Silva, A.W., Vranken, W.F., 2012. ACPYPE - AnteChamber PYthon Parser interfacE. BMC Res. Notes 5, 1–8. https://doi.org/10.1186/1756-0500-5-367.

Swalwell, H., Latimer, J., Haywood, R.M., Birch-Machin, M.A., 2012. Investigating the role of melanin in UVA/UVB- and hydrogen peroxide-induced cellular and mitochondrial ROS production and mitochondrial DNA damage in human melanoma cells. Free Radic. Biol. Med. 52, 626–634. https://doi.org/10.1016/j.freeradbiomed.2011.11.019.

Trott, O., Olson, A.J., 2009. AutoDock Vina: Improving the speed and accuracy of docking with a new scoring function, efficient optimization, and multithreading. J. Comput. Chem. 31, NA-NA. https://doi.org/10.1002/jcc.21334.

Vagula, J.M., Visentainer, J.V., Lopes, A.P., Maistrovicz, F.C., Rotta, E.M., Suzuki, R.M., 2019. Antioxidant activity of fifteen seeds from fruit processing residues by different methods. Acta Sci. - Technol. 41, 1–8. https://doi.org/10.4025/actascitechnol.v41i1.35043.

Vera, K., Raif, A., Ikhtiari, R., 2019. Antioxidant and Anti-elastase Activity of Seed and Peel Extract of P. edulis. Am. Sci. Res. J. Eng. Technol. Sci. 53, 43–48.

Wang, J., Wang, W., Kollman, P.A., Case, D.A., 2006. Automatic atom type and bond type perception in molecular mechanical

calculations. J. Mol. Graph. Model. 25, 247–260. https://doi.org/10.1016/j.jmgm.2005.12.005.

Wen, S.Y., Chen, J.Y., Chen, C.J., Huang, C.Y., Kuo, W.W., 2020. Protective effects of galangin against H2O2-induced aging via the IGF-1 signaling pathway in human dermal fibroblasts. Environ. Toxicol. 35, 115–123. https://doi.org/10.1002/tox.22847.

Wiegand, C., Raschke, C., Elsner, P., 2017. Skin Aging: A Brief Summary of Characteristic Changes. In: Textbook of Aging Skin. Springer, Berlin Heidelberg, pp. 55–65.

Wittenauer, J., MäcKle, S., Sußmann, D., Schweiggert-Weisz, U., Carle, R., 2015. Inhibitory effects of polyphenols from grape pomace extract on collagenase and elastase activity. Fitoterapia 101, 179–187. https://doi.org/10.1016/j.fitote.2015.01.005.

Würtele, M., Hahn, M., Hilpert, K., Höhne, W., 2000. Atomic resolution structure of native porcine pancreatic elastase at 1.1 Å. Acta Crystallogr. D Biol. Crystallogr. 56, 520–523. https://doi.org/10.1107/S0907444900000299.

Yang, E.S., Hwang, J.S., Choi, H.C., Hong, R.H., Kang, S.M., 2008. The effect of genistein on melanin synthesis and in vivo whitening. Korean J. Microbiol. Biotechnol. 36, 72–81.

Zhang, Q., Grice, J.E., Li, P., Jepps, O.G., Wang, G.J., Roberts, M.S., 2009. Skin solubility determines maximum transepidermal flux for similar size molecules. Pharm. Res. 26, 1974–1985. https://doi.org/10.1007/s11095-009-9912-4.